STUDY OF HIGH STRAIN RATE BEHAVIOUR OF ALUMINUM ALLOY UNDER DYNAMIC LOADING USING SPLIT HOPKINSONS PRESSURE BAR(SHPB) AND COMPUTATIONAL TECHNIQUES

A Thesis Submitted in Partial Fulfilment of the Requirement for the Award of the Degree of

MASTER OF ENGINEERING

in CAD CAM Engineering

Submitted By

ANMOL BHATNAGAR

801684002

Under Supervision of

Dr. Devender Kumar

Assistant Professor

Department of Mechanical Engineering

MECHANICAL ENGINEERING DEPARTMENT
THAPAR INSTITUTE OF ENGINEERING & TECHNOLOGY
(A Deemed to be University), PATIALA, PUNJAB
AUG, 2018

CERTIFICATION

This is to certify that the work down in this thesis report title **"Study of High Strain Rate Behavior of Aluminum Alloy Material Under Dynamic Loading Using Split Hopkinsons Pressure Bar(SHPB) and Computational Techniques"** submitted in partial fulfillment of requirement for the award of Master of Engineering Degree in CAD/CAM Engineering in the Mechanical Engineering Department of Thapar Institute of Engineering & Technology, is an authentic record of work carried out by me under the guidance of Dr. Devender Kumar, Assistant Professor, Mechanical Engineering department, Thapar Institute of Engineering & Technology, Patiala. The matter embodied in this report has not been submitted in any part or full to any other university or institute for the award of any degree.

Date: 30th Aug, 2018

Anmol Bhatnagar
Roll No. 801684002

This is to certify that above declaration made by the student concerned is correct to the best of my knowledge & belief.

Date: 30th Aug, 2018

30/07/18

Dr. Devender Kumar
Assistant Professor,
MED, TIET

ACKNOWLEDGEMENT

I would like to express my most profound appreciation to all those who provided me with the possibility to complete this report. Special gratitude to my guide Dr Devender Kumar, whose contribution in stimulating suggestions and encouragement, helped me to coordinate the project especially in writing this report. I would like to thank Dr. Suresh Kumar, Research Associate, TBRL, DRDO, Chandigarh for their invaluable contribution in providing experimental data and guidance through my research work. Furthermore, I would also like to acknowledge with much appreciation the crucial role of my classmates whom all have contributed with something unique and valuable. My heartiest gratitude for my respected parents, for their invaluable love and encouragement at every step of my life.

I further want to express my gratitude to all the T.I.E.T fraternity. T.I.E.T provided me with the infrastructure, knowledge and attitude required for the research.

(Anmol Bhatnagar)

M.E (CAD/CAM Engineering)

Abstract

The intent of the present study is to study the stress-strain characteristics of aluminum alloy(LM-13) at high strain rates and different combinations of length and diameter of the specimen using Split Hopkinsons Pressure Bar (SHPB). This apparatus comprises of a short cylinder-like specimen sandwich between two long slender bars. A compressive stress wave is generated by hitting the end of a bar and the wave immediately begins to traverse towards the specimen. The mechanism involved in the apparatus is well explained in the thesis. By tracking the strains in the two bars using different instruments, stress-strain properties of the specimen can be determined. A 3D finite element model was generated in ANSYS and was simulated at very high strain rates as in the experiments to explore the dynamic behavior of the aluminum specimen.

Three different materials were compared for better validation. Experimental results used for present study are having diameter less than the diameter of the incident/transmitting bars of the SHPB machine. A conventional SHPB setup can only test on the specimen with length and diameter less than 20mm. Four combinations of length and diameter were tested at high strain rate while keeping the length constant at 20mm in one set and 24 mm in the other set with increasing the diameter from 20 to 32 mm in ANSYS at very high strain rate to establish a study for the impacts greater than 20 mm in diameter. The model was validated with the help of literature and experiments conducted on SHPB setup. A particular case of metal matrix composite (MMC) specimen was also taken from the literature and modelled in ANSYS and results were compared with the experiment. Based on the comparison study, cogency, applicability and accuracy of simulation was ensured for samples with large diameter.

Keywords: Split Hopkinson Pressure Bar, ANSYS, High strain rate (HSR), Simulation

Table of Contents

List of Figures

List of Tables

Nomenclature

x,y,z	Cartesian coordinates
u,v,w	In plane displacements
T	Temperature
E	Young's Modulus
ν	Poisson's Ratio
σ_1 , σ_2	Principal Stresses
ε_1, ε_2	Strain Rates
C_{bar}	Mean Bar wave velocity

Acronyms

FEM	Finite Element Method
HEMPDS	Hyper Element Meshing and Part Designing Software
SHPB	Split Hopkinsons Pressure Bar
ANSYS	Analysis System
MMC	Metal Matrix Composites

Chapter 1 Introduction

1.1 Motivation and Background

Ballistic Materials are presented to different effects because of blast caused by individuals purposefully or inadvertently. In this manner materials which have dangers from blasts ought to be impact safe. Due to this, the stress-strain characteristics of different sample of variety of materials at high-strain rates need to be investigated. Split Hopkinson Pressure Bar (SHPB) is widely used test setup which has given huge outcomes at high-strain rate. In SHPB, materials can be tested at different strain rates in the scope of 10 to 10000 s^{-1}. Since engineering design considerations for materials used in everyday life are quite lower than that used for armors and regular materials are not blast resistant amid a blast and are prone to be damaged from blast. Outline of impact safe materials is considered as a particular field of research and application. In general, mechanical designer and basic architects don't know about a large portion of the ideas in regards to outline of impact safe structures. This field is principally restricted to defense segments. This designing and building information can upgrade the new and existing materials to alleviate the impacts of a blast.

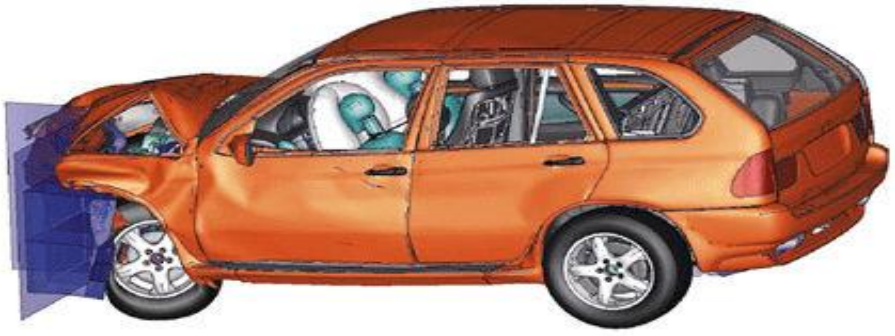

Fig.1.1: Simulation of car impact test [www.artstor.org (accessed September 1, 2017)]

1.2 Ballistic Tests

Prior to a particular armortype and configuration is chosen to give the coveted insurance to anarmored vehicle, sample of the protective material must be subjected to the foreseen assault condition. The most vital of these condition is the assault by Kinetic Energy (K.E) projectiles. Throughout the years, much endeavors have been coordinated towards building up the ideal testing strategies to give a quantitative measure of the capacity of protective layer to oppose

aperture by K.E. projectiles and to gauge the likelihood that a shot will puncture the shield of a framework under test.

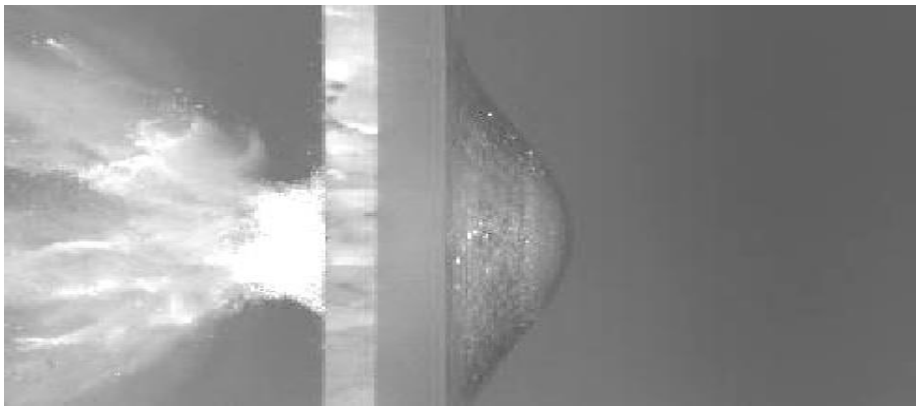

Fig. 1.2 : High speed image of a .44 Magnum bullet impact on a glass sheet[www. Researchgate.net (Accessed sept 3, 2017)]

Ballistic resistance testing routinely utilizes sensitive and exceptionally costly exploratory methods where consecutive test outlines are utilized to evaluate a specific quantile of the likelihood of puncturing. In the current monetary climate of sequestration and spending shortages, proficiency is basic for test and assessment. Notwithstanding the worry about whether a specific sort of assault will or won't overcome a protective layer target, it is additionally critical on account of annihilations to realize that to what degree the defensive layer was crushed. Nonetheless, it has just been the previous decade, there is a critical information handling upgrades in high-strain rate testing. The SHPB is a device outlined primarily for the materials need to be test at variable strain rate in the scope of 10 to 10000/sec.

1.3 Split Hopkinsons Pressure Bar

The Split Hopkinsons Pressure Bar comprises of four noteworthy segments Striker, Incident bar, Specimen and Transmitter bar. The sample is positioned in between the two bars i.e., incident and transmitter bar. The gas gun (sticker) applies a high-impact force at one end of the incident bar creating compressive stresses. The shock wave travels in a uni-axial direction into the incident bar which then reaches the interface of the incident bar and specimen.

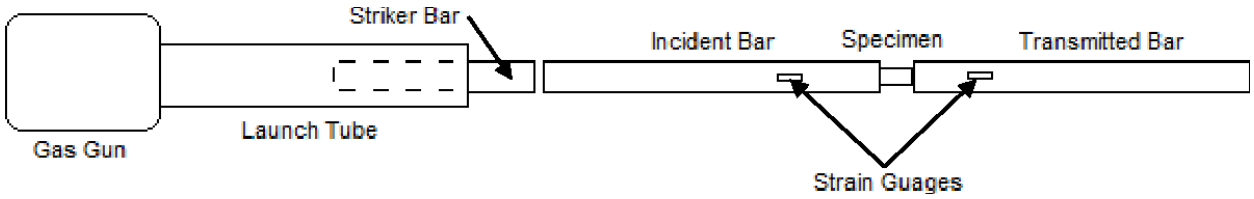

Fig. 1.3: Basic Layout of SHPB[Chen, 1987]

A portion of the shock wave is reflected back as a wave creating tensile effect which pass through incident bar while the rest keeps on propagating into the transmitter bar as a pressure wave. The SHPB has two particular highlights that are not quite the same as an ordinary material testing machine. First difference is in its stiffness. Bars with moderately little width SHPB are not drastically stiffer than the specimen (Chen,2001), as opposed to axis stiffness of average massive loading in hydraulic or screw-driven testing machines. The other distinction is that the SHPB bar didn't have a shut circle criticism control framework for constant observing and change of the stacking conditions being connected to the example. The versatile poles are additionally known as input bar and yield bar, individually, by numerous researchers (Clausen,2011) In this arrangement, with impact of input bar through striker, for example, a hit of mallet, a compressive pressure wave is produced and after that spreads into the incident and therefore in sample, moving the incident bar towards the sample as it clears by. At the point when it reaches at the interface between the input bar and the sample, some portion of the wave is reflected again into the input bar towards the front and the rest transmits through the sample into the transmission bar. Instrumentations in the laboratory can record the pressure waves in the incident bar proliferating towards the sample and being reflected once again from the sample and the wave in the transmission bar with the assistance of strain gauge arranged at the center of incident and transmission bar as appeared in the figure 1.3. The voltage signals from strain gauge passes through a signal conditioner to amplify the signal which thus is passed to a Digital Oscilloscope. Under this course of action, the effect is controllable and quantitative in nature. The velocity of impact and size of the sample can be selected suitably to accomplish distinctive strain rates. Terminal Ballistic Research Laboratory (TBRL), Chandigarh, India is working on testing of aluminum combination (LM-13) material for structural and armor applications.

Chapter 2 Literature review

2.1 History of Split Hopkinsons Pressure Bar.

Material properties, for example, yield pressure and ultimate strength, recorded within design handbooks and manuals, are acquired under quasi-static stacking specifications utilizing normal testing parameters with the assistance of standard testing methods. To guarantee the quality and dependability of the item under effect conditions, for example, those experienced in the vehicle crash, and sports impact, the mechanical responses of materials under such stacking must be computed exactly. Be that as it may, high-rate stacking conditions are beyond the extent of ordinary material testing machines. To acquire the dynamic reaction of materials under lab controlled conditions, (Kolsky,1949) tackled these issues with an extremely novel arrangement. Rather than the coordinate effect on the test sample, the set of two elastic bars on the two sides of the sample and after that it struck towards one bars having an explosive impact. The idea is schematically shown in Fig. 2.1.

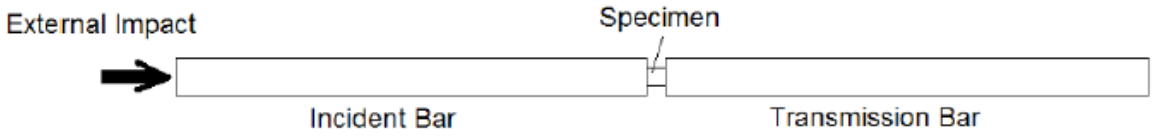

Fig. 2.1: Basic design of KolskyBar[Kolsky, 1949]

The pressure variant of the Kolsky bar is the first setup built by Herbert Kolsky (1949). The Kolsky bar in pressure is likewise generally called a Split-Hopkinson pressure bar (SHPB) in remembrance of John Hopkinson and his son, Bertram Hopkinson. John Hopkinson(1872) directed rupture test on a wire of iron by the effect of a suspended weight. The schematic of this investigation is shown in Fig. 2.2.

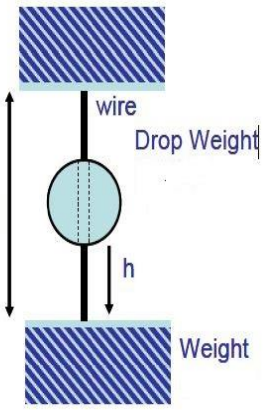

Fig 2.2: John Hopkinsons Experiment Setup[Hopkinsons, 1872]

The failure of the wire was located on either side of incident end or the suspended end contingent upon the speed of impact, however paying little respect to the mass of the weight. This test initially uncovers the spread of pressure waves in the arrangement, in any case, it was extremely challenging to quantify pressure wave proliferation in the nineteenth century. Bertram Hopkinson (1914) imagined a weight bar to gauge the weight created by high explosives or rapid effect of bullets(figure. 2.3).

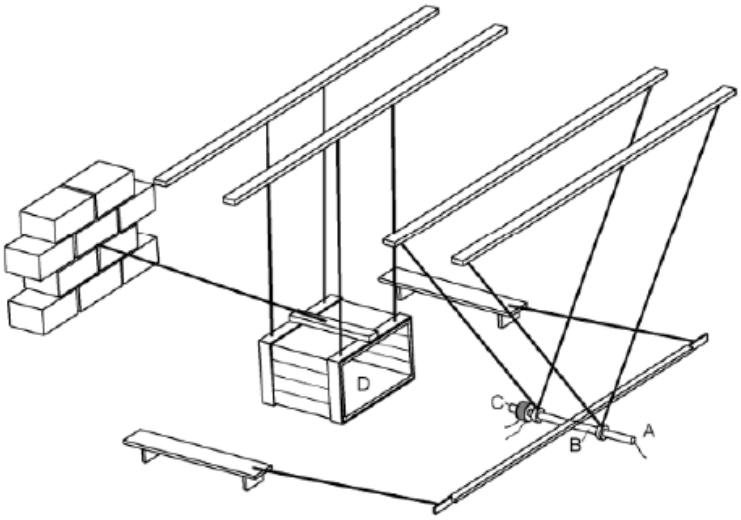

Fig 2.3: Bertam Hopkinsons Experimental Setup[Kolsky, 1949]

As appeared in figure 2.3, Bertram Hopkinson (1914) utilized pendulums with tracing mechanism to record the developments of bars. The energy of a chamber (B) affected by explosion of the firearm stricker (A) and a minute bar (C) appended to the opposite end of B by attraction from magnet was figured, which was a measure of the weight produced by the explosion. At the point when C has shorter length than half of the movement separation of stress

wave over the stacking term, both C and B would take off. C's length expanded until the point when B was very still in the wake of stacking. Just C took off. The stacking beat length was the round-trip time for the pressure wave going in C. In any case, the estimations were inexact in nature because of the simple constrained measurement methods around then.

2.2 Computer Modelling and Mathematical formulation of Split Hopkinson Pressure Bar

In the previous two-decade broad work has been done on displaying and recreation of SHPB. Numerous researchers extemporized the Hopkinson bar test by availing high bandwidth flag analyzers, high-speed computer systems, a storage arrangement, which supports to get more exact outcomes having good resolutions. After improvement of the Hopkinson's test setup more researchers attempted to consider the characteristics of both bars, sample's effects generated through geometry and its computer simulation. Be that as it may, a few scientists have worked widely on metals and some on non-metals

2.2.1 Non metallic Materials

Ravichandran *et. al.* (1996) performed dynamic multi-axial loading on the glass ceramic, Macor under the quasistatic condition within the confining pressure range of 10-23 MPa. They also proposed compressive mechanism of rupture for brittle materials using medium lateral confinement.

Meng *et. al*. (2002) utilized the SHPB procedure to gauge the dynamic strength enhancement of solid like materials at high strain-rate in the vicinity of 101 and 103 s^{-1} by Finite Element and Drucker-Prager strategy. Reliance of Dynamic Increase factor(DIF) on various Strain rates. DIF is essentially the proportion of Dynamic Strength to quasi-static quality. DIF was considered as an essential parameter to gauge the strain – rate impact on the quality of the solid-like material. It was watched that there is an expansion in unique quality and accordingly expressed that solid is a strain-rate sensitive. Numerical recreations demonstrate that the horizontal idleness power of the example builds the parallel control in SHPB test, which causes an obvious increment of the DIF for concrete

Song *et al.*(2007) discussed the dynamic fracture of ceramic material after slight modification in the SHPB by introducing quartz back panel as shown in figure 2.4(a). It was observed that specimen begins to fail at 70 μs and 5200MPa.

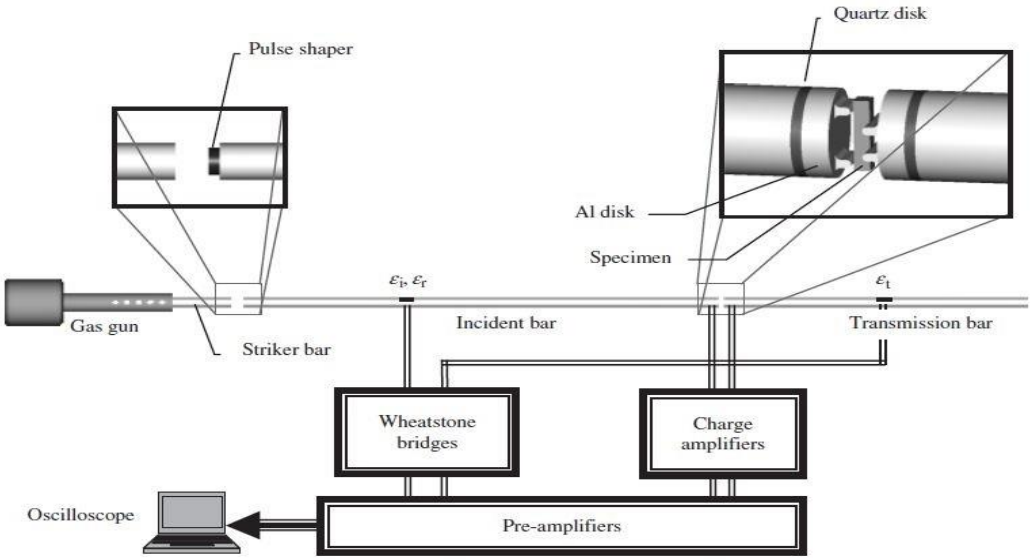

(a) Schematic Diagram of the SHPB setup with quartz disk [Song *et al.* 2007]

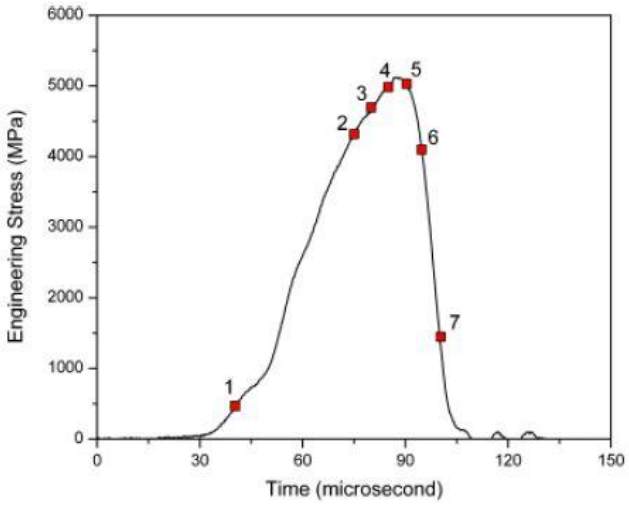

(b) Axial compressive stress history of the specimen [Song *et al.* 2007]

Fig. 2.4: (a) Schematic Diagram of the SHPB setup with quartz disk and (b) Axial compressive stress history of the specimen [Song *et. al.* 2007]

Wang *et. al*. (2012) considered the mechanical behavior of fiber-strengthened high quality concrete(FRHSC) with quality between 80-90MPa utilizing SHPB at strain rates from 40 to $300s^{-1}$.Fracure example were likewise talked about for sample, solid lattice and filaments, It was watched that DIF for FRHSC was expanded with strain rates going from 40-300s-1 and toughness of the solid was additionally increased with strain rate.

Ren *et. al*. (2014) contemplated the quasi-static and dynamic mechanical behaviors of ceramic resin fiber constrained concrete (CRFRC) through a 100mm dia SHPB framework. It was watched that the quasi-static compressive, part pliable and flexural strength of CRFRC increment with the ascent of fiber volume fraction and adding of ceramic fiber to plain concrete can altogether enhance its properties like strength, critical strain, and energy absorption.

Salloum *et. al.* (2014) detected the dynamic conduct of annular and strong solid samples utilizing SHPB at high strain rates extending from 50-300s^{-1}. It was observed that the mode of failure of concrete specimen was a typical ductile failure at high strain-rates and brittle at low strain-rates, Higher estimations of strain-rate were watched for tests with bring down estimation of length to external distance across proportion.

Mishra *et. al*. (2017) tested Himalayan quartzite tried the dynamic pressure strain reaction under high stacking rates extending from 49s-1 to 316 s-1 through uniaxial compressive 38mm distance across utilizing SHPB. The dynamic pressure strain reaction, top pressure, elastic modulus and power balance at the incident and transmission bar ends of the stone example are considered. The physical properties and static pressure strain conduct of the stone are additionally explored. The peak stress increments at a rate of 22% from low (77 s^{-1} to 94 s^{-1}) to medium (134 s^{-1} to 215 s^{-1}) strain rate and by 37.7% from medium (134 s^{-1} to 215 s^{-1}) to high (260 s^{-1} to 316 s^{-1}) strain rate. The flexible modulus of quartzite does not demonstrate a specific pattern with expanding strain rate. The dynamic compressive pressure 669.297 MPa at 316 s^{-1} is about six times of static compressive pressure.

2.2.2 Metallic Materials.

Charles *et al.* (1994) performed numerical simulations of the Split-Hopkinson pressure bar (SHPB) experiments have been performed using the two-dimensional wave propagation computer program HEMPDS. This was the first ever research paper which introduced numerical simulation of a SHPB. The numerical results were then compared against experimental data as shown in figure 2.6.

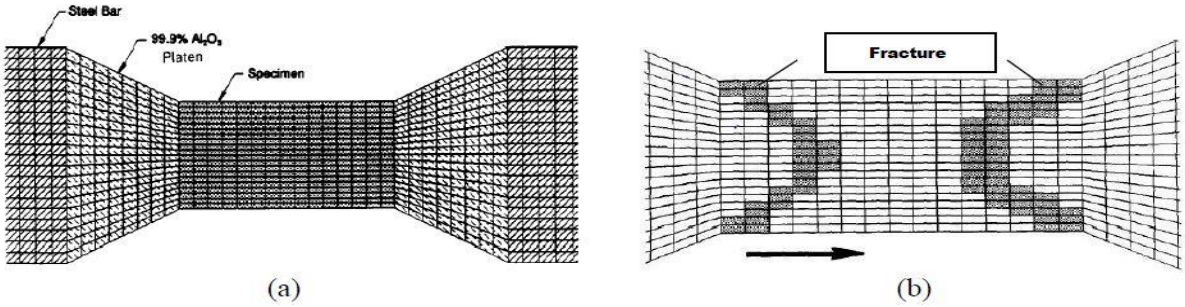

Fig. 2.5: Finite Element Model of the specimen (a) Before and (b) After the loading [Charles *et. al.* 1991]

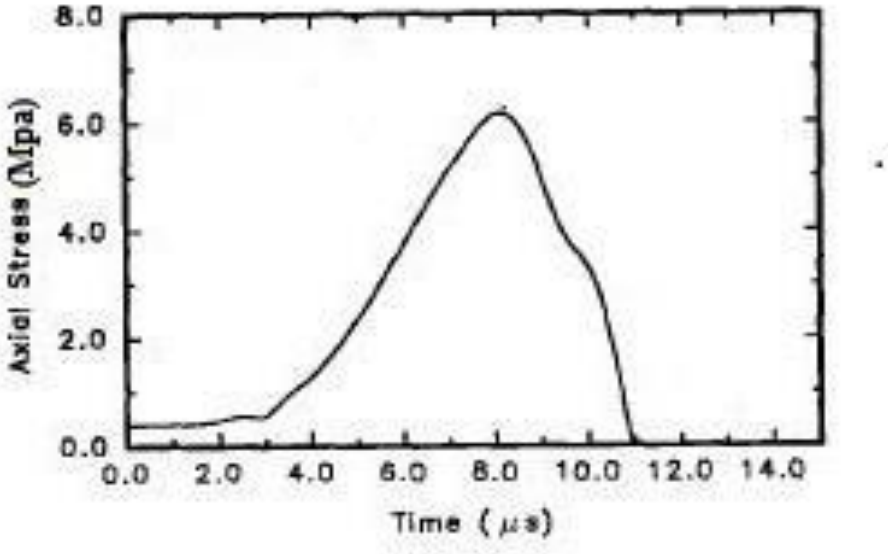

Fig. 2.6: Axial Stress vs Time Plot [Charles *et. al.* 1994]

Chen *et. al.* (2001) obtained compressive high strain data of limestone after slightly modifying SHPB setup by placing a thin copper disk between incident and striking bar, after the impact of the striker on the copper disk a nondispersive ramp pulse propagates in the incident bar and produces a nearly constant strain rate in the limestone sample. A FEM model was also generated in FEMtools 2.0 to simulate the impact on the sample and was verified by the experimental data.It was observed that stress pulse is nearly a linear ramp for about 60 μs and has a stress-loading rate of about 2.5MPa/μs. In figure 2.6 , strain rate is nearly constant for 15μs $< t <$ 50μs. At about 50 μs, the limestone stone sample begins to fail and the range of the trial is over.

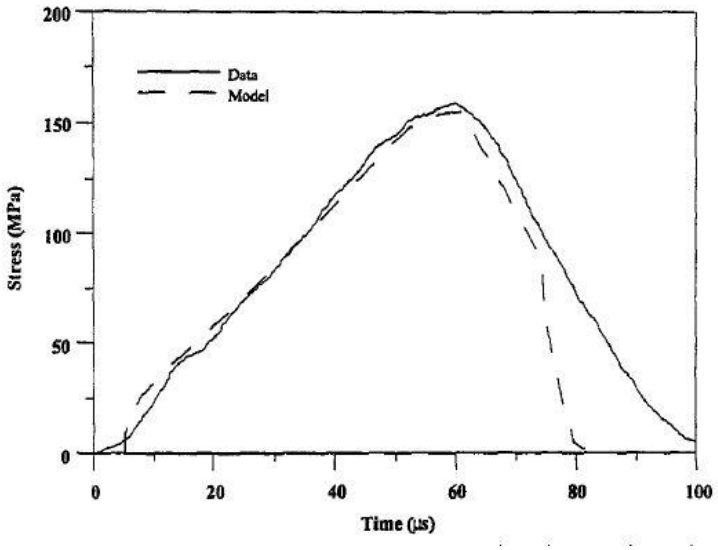

Fig. 2.7: Experimental and Model prediction of limestone sample [Chen *et. al.* 200]

Zheng *et. al.* (2004) calculated the dynamic stress-strain relation of the alumina with alternate dense and porous layers with the help of experimental method and simulation. AKP 30 alumina powder with an average particle size of 0.3 μs were used as the raw material and Polymethyl methacrylate (PMMA) powder were added for generating porous layer with an average size of 70μs.

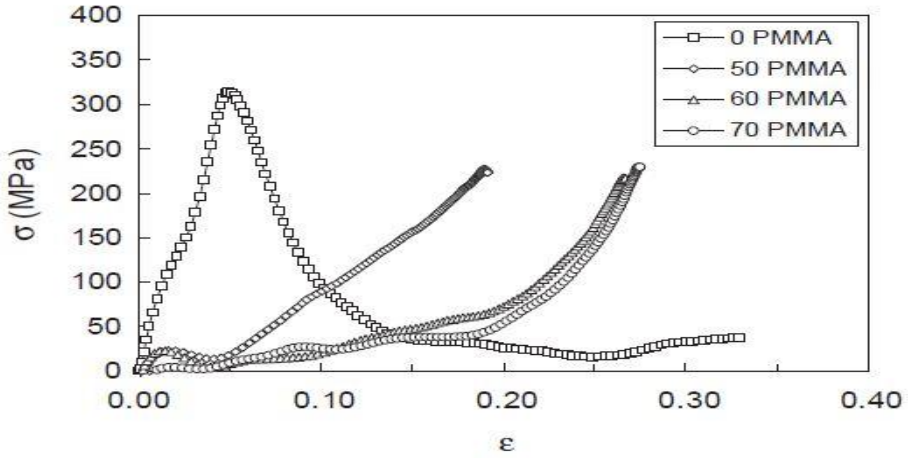

Fig. 2.8: Stress-strain curves of the sample with different volumes of PMMA added at strain rate of 3500 s^{-1} [Zheng *et al.* 2004]

Rodriguez et al. (2004) contemplated the stress strain conduct alumina-zirconia doped with CuO and TiO2 at the temperature extending between 900-1200ºC. Strain rate was checked by the equation

$$\varepsilon' = A\frac{\sigma^n}{dp}exp\left(-\frac{Q}{RT}\right) \quad (1)$$

Where *A* is a constant, σ is the stress, *d* is the grain size and *T* is the absolute temperature; *n, p* and *Q* are, respectively, the stress exponent. At 1100ºC, destabilization of the material was seen, one of the conceivable reason is change in oxidation condition of the copper in arrangement, changing from Cu^{2+} to Cu^{1+}. It displays genuine stationary plastic deformation characterstics.

Ravichandran*et al.*(2005) conducted series of plate impact experiment on highly porous Al_2O_3 ceramic at the loading stress rates ranging from 1.6MPa to 4.2MPa. It wasobserved that materias are more effected by particle size when rate of loading is low and becomes less effected when the rate of loading becomes higher and higher.

Adrian *et al.*(2007) studied the dynamic impact on copper specimen in the presence of an oil film between incident bar and specimen with the help of experiment and simulation in LS-Dyna.

(a)

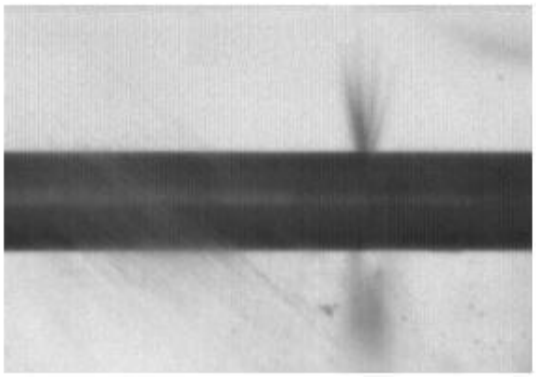

(b)

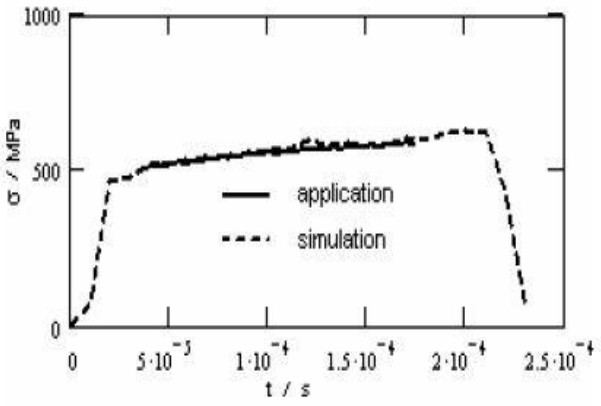

Fig. 2.9 : (a) Oil film Ejection after impact and (b) Stress resulted from experiment and (contd.) simulation [Adrian *et al.* 2007]

Guden *et al.*(2009) determined the compressional deformation of a 316L metallic sample comprissed of aluminium metallic hollow spheres(MHS) both numerically and experimentally. The tested sphere sample displayed greater crushing stress value when the strain rate increased from quasi-static($0.8x10^{-4}$ s^{-1}) to high strain rate (600 s^{-1}).

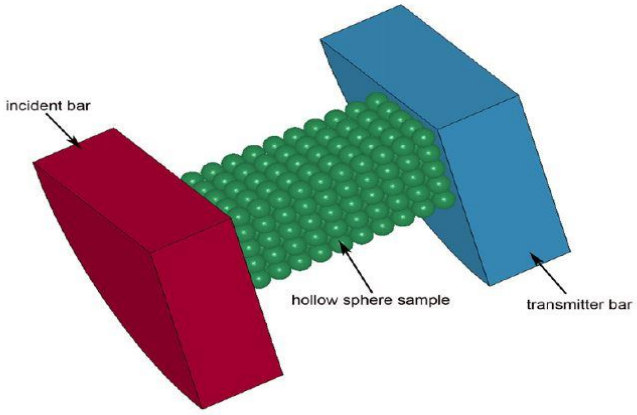

Fig.2.10: Numerical model of the MHS between the bars [Guden *et. al.* 2009]

Bobbili *et al.* (2014) demonstrated the use of Artificial neural network (ANN) to generate a constitutive model for high strain rate impact on high strength tempered steel. The specimen was tested at 1000 s^{-1}, 2000 s^{-1}, 3000 s^{-1} and 4000 s^{-1} . Based on Experimental and simulation data a rapid increase in yield stress has been occurred with the increase in strain rate.

Lu *et al.*(2014) considered the influences od some factors such as inertia, friction, punching and elastic wave dispersion in SHPB tests and mainly focused of interfacial effects of friction for 4 different type of materials i.e. silicone rubber, PU foam, PBX-HMX and 6061-T6 Al alloy were tested by the SHPB under three different interfacial friction condition of lubricated, dry and bonded surfaces.

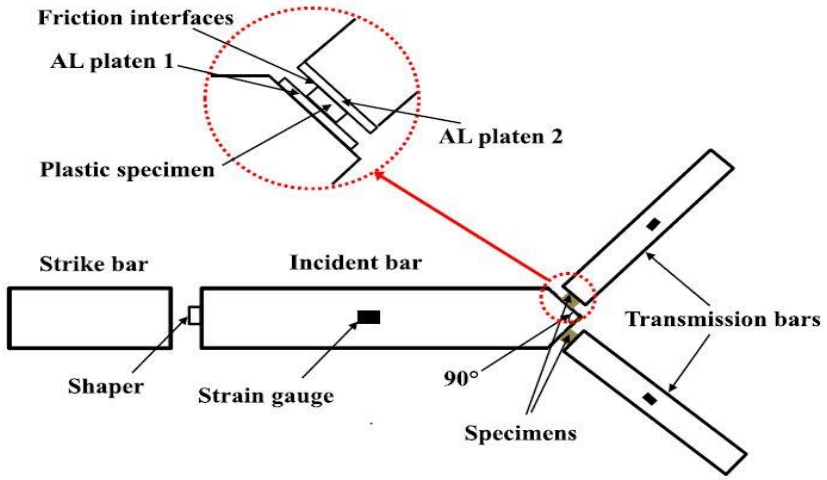

Fig. 2.11: Test Setup including frictional interfaces [Lu *et. al.* 2014]

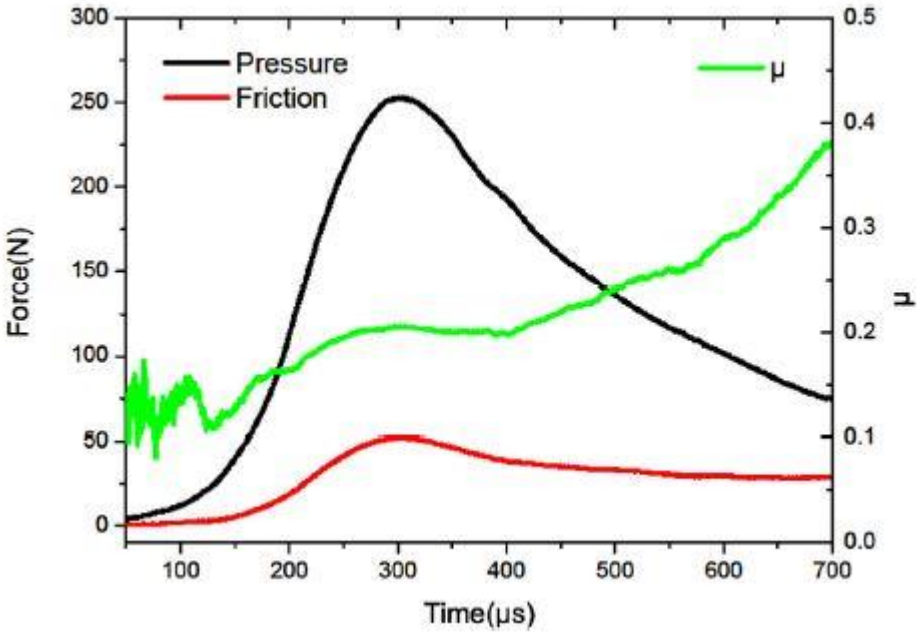

Fig. 2.12: Rate of change of Friction and Pressure w.r.t. time[Lu *et. al.* 2014]

Presented data give an insight that force of friction varies with change in radius of the sample and the interfacial friction coefficient changes during the process of loading.

Aradhye *et al*. (2017) conducted high strain experiments on A356/Al_2O_3 Aluminum Combination Metal Matrix Composites(MMCs) with 0, 4, 8, and 12% fiber volume division of aluminum oxide(Al_2O_3) and were tentatively and numerically portrayed with SHPB test setup

utilizing Ls-Dyna. Dynamic pressure strain conduct was acquired at various strain rates going from $100s^{-1}$ to $1200s^{-1}$. It was watched that expansion in fiber volume division brought about reduction of peak stress in sample.

Hu *et. al.* (2017) estimated the disengagement thickness and mechanical limit stress(MTS) of without oxygen high warm conductivity(OFHC) copper stacked at strain rates in the scope of 10^2 to 10^6 s^{-1} were estimated. The separation densities of OFHC copper tests subjected to $\varepsilon = 0.0325$ (500 s^{-1}, 0.1 GPa), $\varepsilon = 0.0834$ (900 s^{-1}, 0.17 GPa), $\varepsilon = 0.111$ (1800 s^{-1}, 0.20 GPa), and $\varepsilon = 0.229$ (3000 s^{-1}, 0.28 GPa) SHPB stacking were $1.83x10^{14}$, 5.43x1014, $6.79x10^{14}$, and $2.12x10^{15}$ m^{-2}, individually. The relating mechanical threshold stresses were 70, 149, 185, and 298 MPa, respectively.

2.3 Gaps in literature

In most of the literature in past years have only analyzed one or more materials under a handful combination of L/D ratio under SHPB test. Furthermore, SHPB only gives results on a confined area (upto 20mm dia) of a test specimen, but in real application the impact of a bullet creates way larger cavity than 20 mm. The analysis of the impacts greater than 20 mm have not yet been analyzed in any literature.

2.4 Objectives of the Present Work

- To Analyze the strain rate for aluminum alloy (LM-specimen in a FE solver for various combinationsof L/D ratio of the specimen.
- To validate strain rate data obtained from simulation with that of experimental data.
- To analyze the suitability of larger specimens by extrapolating the results for L=20mm alongwith different values of diameter i.e., D=20, 24, 28 and 32mm.

3.1Aluminum(LM-13)

Aluminum alloy has always been the good choice throughout the world because aluminum alloy has light weight, cost effectiveness and advancements in processing over the years make it highly acceptable as structural material applications in various industries and defense sector. Compressive stress-strain curves of aluminum alloy were studied in the strain rate ranging from 2000 to 5800 s^{-1}. In the present work, room temperature SHPB is used to study the compressive stress-strain characteristics of aluminum alloy samples. Aluminum alloy materials observed to be the best option with its one of a kind limit of outlining the material to give required properties. Aluminum alloy composites are increasing far reaching acknowledgment for aviation application in view of their high strength and density. In the present work, an endeavor is made to get ready and concentrate the mechanical properties of Aluminum LM13 – MgO particulates Composite. The Aluminum LM13– MgO particulates having 2wt%, 4wt%, 6wt%, 8wt% and 10wt% were manufactured by stir casting technique. The ingots were subjected to T6 Heat treatment to upgrade the properties. The composite samples were machined according to ASTM test benchmarks. The microstructures of the composites were concentrated to know the scattering of the MgO particulates in Matrix. It has been watched that expansion of MgO particulates essentially enhances extreme rigidity alongside compressive and hardness strength as contrasted and that of unreinforced composite.

3.2 Wave Propagation in SHPB

As talked about in the first chapter the setup for Split Hopkinsons Pressure Bar is made up of two bars i.e., incident and transmitting bar, with a settled cross-sectional are A_{bar} ,Young's Modulus E_{bar} , and density ρ_{bar}. For building up the administered condition of axial vibration it is just important to take one of them into consideration since the two bars are indistinguishable. 1.5 is the normal proportion of Length and Diameter of Hopkinsons Bar which is taken during studies.

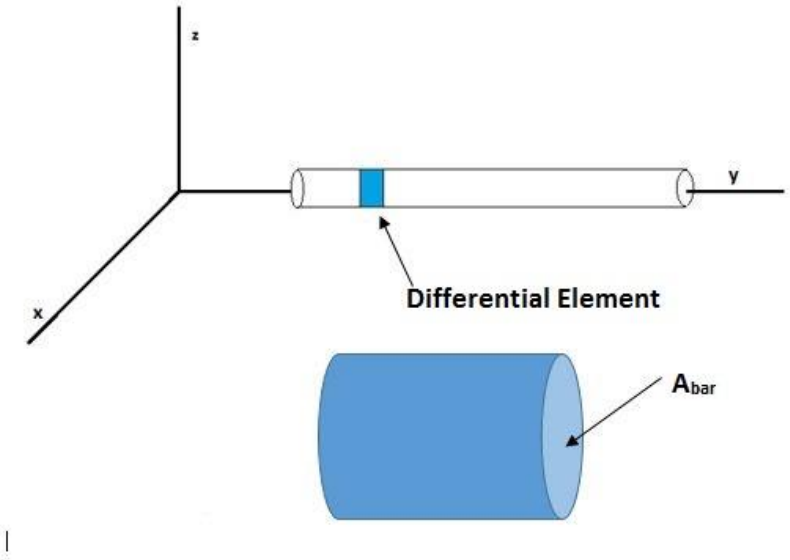

Fig.3.1: Un-deformed bar and differential element

The result calculation for SHPB setup starts after selection of a differential cross sectional area which is part of a bar. Fig. 3.2 demonstrates the pressure bar which is non-distorted alongside a differential component.

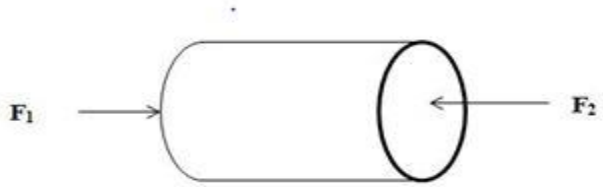

Fig. 3.2: Differential Element in compression

$A_{ba\,r}$ and *dy* is the area and length of the differential component considered. Before impacting, the bar stays in equilibrium. When it is impacted, the differential element encounters pressure because of powers $F_1$and F_2, as appeared in figure 3.2.

In the differential element, the forces associated with stresses generated on the element cross-section are counter–compression in nature. There is a stress-strains relationship includes Elastic modulus of bar, which follows Hooke's law. However, strains can be combined and termed with the help of element displacement. In order to restrict compression, the forces involved in element displacements (*u)* are as follow:

$$F_y = A_{bar} E_{bar} \frac{\partial u}{y} \quad (2)$$

Which is expected as uniaxial condition of pressure. This axis constrains acting ordinary to the zone of cross-section of the differential component which is plainly noticeable in figure 3.2 gives the magnitude of this power

Utilizing Newton's second law (*F=m.a)* the loads following up on the component are collectively produce at the accompanying condition clarifying the movement of the pressure waves

$$A_{bar}E_{bar}\frac{\partial u_2}{\partial y} - A_{bar}E_{bar}\frac{\partial u_1}{\partial y} = A_{bar}dy\rho\frac{\partial^2 u_1}{\partial t^2} \quad (3)$$

In this equation, it is assumed that particle acceleration remains equal at every point of differential element. When the above equation is solved, we get

$$C_{bar}^2\left[\frac{\partial u_2}{\partial y} - \frac{\partial u_1}{\partial y}\right] = \frac{\partial^2 u_1}{\partial t^2}dy \quad (4)$$

Where C_{bar} is the velocity of wave(Chen et al, 2005), can be calculated from

$$C_{bar} = \sqrt{\frac{E_{bar}}{\rho_{bar}}} \quad (5)$$

Where E_{bar} and ρ_{bar} are the bar young's modulus and density, separately. This condition of movement can be rearranged by discovering relations between the removals on one side of the differential components to the relocations of the opposite side which is

$$u_1 = u_2 + \frac{\partial u_1}{\partial y}dy \quad (6)$$

There is an assumption that is equal change in displacement rate on each face of the element, which probably due to differential element. Differentiation give

$$\frac{\partial u_2}{\partial y} = \frac{\partial u_1}{\partial y} + \frac{\partial^2 u_1}{\partial y^2}dy \quad (7)$$

Now equation of motion becomes:

$$C_{bar}^2\left[\frac{\partial u_2}{\partial y} - \frac{\partial u_1}{\partial y}\right] = \frac{\partial^2 u_1}{\partial t^2} \quad (8)$$

It can be observed that there is minimal utilization of condition of movement in the investigation of hopkinsons bar, yet it supports the hypothetical thought of wave velocity of unknown characteristics, which can be utilized to discover the specimen's, strain and strain rate.

3.2.1 Specimen Stress

The average of stresses in the specimen can be presented in relation of the forces exerted on the surfaces of every sample. Figure 3.3 represents cylindrical sample.

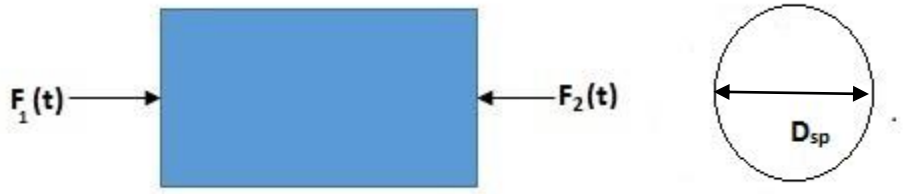

Fig. 3.3: Diagram of specimen with forces

Forces $F_1(t)$ and $F_2(t)$ are exerted on the sample diameter D_{sp} when it is placed within both the bars. Sample bears an average force F_{avg}

$$F_{avg}(t) = \frac{F_1(t) + F_2(t)}{2} \tag{9}$$

Now the average stress on sample is

$$\sigma_{avg} = \frac{F_{avg}(t)}{\frac{\pi D_{sp}^2}{4}} \tag{10}$$

The loads at the ends of the pressure bars for a sample with no other forces actin on it can be coined in terms of the both incident and reflected strains of the pressure bars as equation 11 and 12

$$F_1(t) = (E_{bar}\,[\varepsilon_i(t) + \varepsilon_r(t)])\frac{\pi D_{bar}^2}{4} \tag{11}$$

$$F_2(t) = (E_{bar}\varepsilon_t(t))\frac{\pi D_{bar}^2}{4} \tag{12}$$

Where bar diameter is taken as D_{bar}. Using equation (8),(9) and (11), the average stress in terms of the strain generated in pressure bars is

$$\sigma_{avg}(t) = \frac{D_{bar}^2}{2D_{sp}^2} E_{bar}[\varepsilon_i(t) + \varepsilon_r(t) + \varepsilon_t(t)] \tag{13}$$

If it can be assumed that there is a uniform deformation of the specimen, the strains produced in both the bars can be equated as shown in equation 14

$$\varepsilon_i(t) + \varepsilon_r(t) = \varepsilon_t(t) \tag{14}$$

Therefore, the sample's average stress can be represented as

$$\sigma_{avg}(t) = \frac{D_{bar}^2}{2D_{sp}^2} E_{bar}\varepsilon_t(t) \tag{15}$$

It can be clearly seen from this equation that the specimen stresses are proportional to the strain amplitude spread into the transmitted bar via specimen.

3.2.2 Specimen strain rate and strain.

Strain induces turning i.e., movement, which when detached by time provides speed. From the interfacial velocity of the pressure bar and sample, the sample-strain rate can be calculated. The assurance of the articulation for the specimen's strain rate and strain, the extent that the pressure bar's state of displacement is explored which is shown here for the convenience. Considering the development of the incident bar as u_1 and that of bar of transmission as u_2, it can be written as

$$u_1 = \int_0^t C_{bar}\varepsilon_1(t)dt \tag{16}$$

And

$$u_2 = \int_0^t C_{bar}\varepsilon_2(t)dt \tag{17}$$

The left and right end of the specimen can be referred with the help of subscripts 1 and 2. above Equation (16) and (17) can be altered as a function of the incident, reflected and transmitted wave pulses.

$$u_1 = C_{bar}\int_0^t(\varepsilon_1 - \varepsilon_2)dt \tag{18}$$

$$u_2 = C_{bar}\int_0^t \varepsilon_t\, dt \tag{19}$$

The stress and strain in compression are considered positive. As assumed, the uniformity in the state of strain and stress in the specimen thickness, its strain Es, is given by the expression below

$$\varepsilon_s = \frac{u_1 - u_2}{L_{sp}} \tag{20}$$

Where specimen length is represented by L_{sp}. Eq. (19) and (16) can be substituted into Eqn (20) the strain the specimen is subject to is given

$$\varepsilon_s(t) = \frac{C_{bar}}{L_{sp}} \int_0^t (\varepsilon_i - \varepsilon_r - \varepsilon_t)\, dt \tag{21}$$

With help of equation (15), equation (21) can be written as

$$\varepsilon_s(t) = -\frac{2C_{bar}}{L_{sp}} \int_0^t \varepsilon_r\, dt \tag{22}$$

Equation 23 gives the strain rate

$$\varepsilon' = \frac{2C_{bar}\varepsilon_r}{L_{bar}} \tag{23}$$

Once establishment of equilibrium force has taken place, equation (15), (16), (22) and (23) are valid immediately. When the deformation of the specimen is achieved by just intersecting the point of yield of specimen materials, the following relationship can be satisfied with the help of Hooke's Law

$$\sigma_y = E_{bar}\varepsilon_y \tag{24}$$

Where σ_y is yield stress and E_{sp} is young's modulus of the specimen respectively.

3.3 Numerical Analysis using ANSYS

The Finite element(FE) software ANSYS15.0 has been utilized to reenact the SHPB test on Aluminum alloy material. Characterization of specimens under effect stacking for wide range strain rates requires both numerical and test reenactment of SHPB tests on the sample under uniaxial conditions. It is imperative to think about the numerical reenactment of SHPB experiments on materials considering the elastic and plastic conduct of sample. To foresee the dynamic reactions under the weight adequacy presented by a striker bar on the surface of incident bar following fundamental advances were taken after-

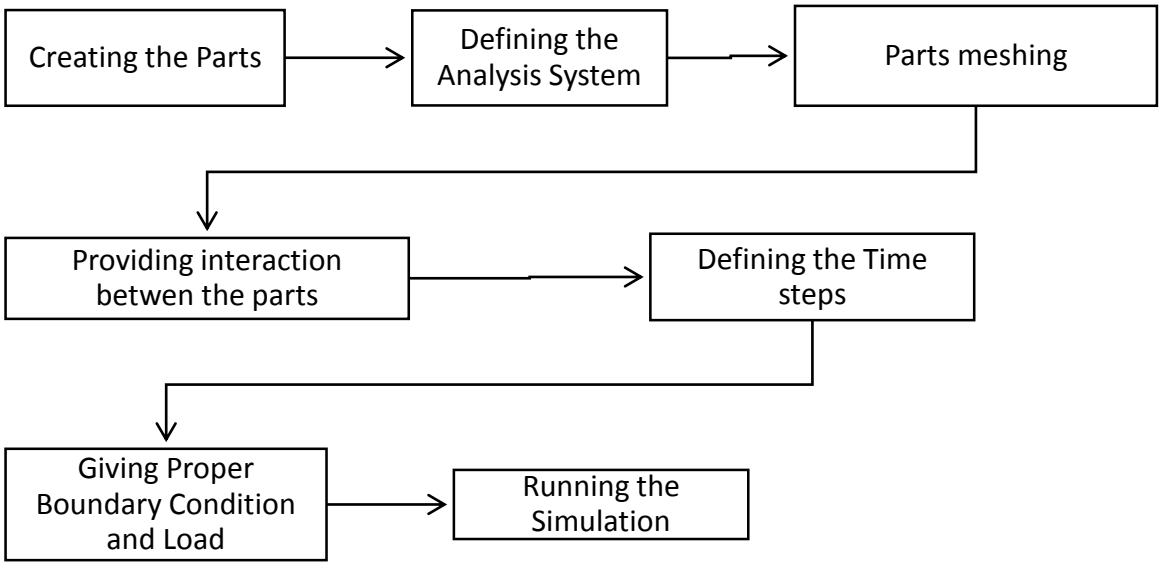

Fig. 3.4: Basic Steps Followed in Pre-processing

1. Creating the Parts

ANSYS Design Modeler was used to create two sets of 4 Combination of Incident Bar, Specimen and Transmitting Bar based on length and diameter of the specimen i.e., 20-20, 20-24, 20-28, 20-32 as shown in the figure 3.5 to 3.8. The material for incident and transmitting bar were taken as High Strength Maraging steel VM350 steel and specimen Aluminum alloy (LM-13). The properties of the transmitting bar, specimen and incident bar are given in the table 1.

Table 1: Properties of the Incident Bar, Transmitting Bar and Specimen

Entity	Diameter(mm)	Length(m)	Mass Density,ρ (Kg/m$^{3)}$	Young's Modulus, E(GPa)	Poisson's Ratio, ϑ
Incident Bar	20	1.5	8100	200	0.3
Specimen	20-24	0.02,0.024	2770	71	0.3
Transmitting Bar	20	1.5	8100	200	0.3

- L=D=20 mm

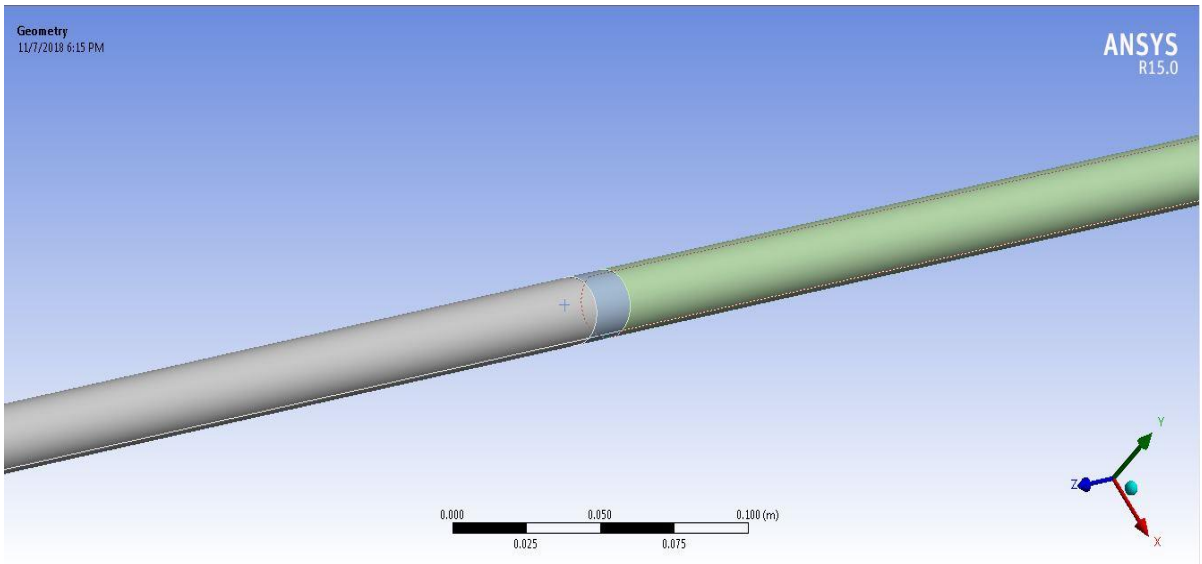

Fig. 3.5: Incident Bar , Specimen(D=20mm) & Transmitting Bar in Ansys Window

- L=20mm and D= 24mm

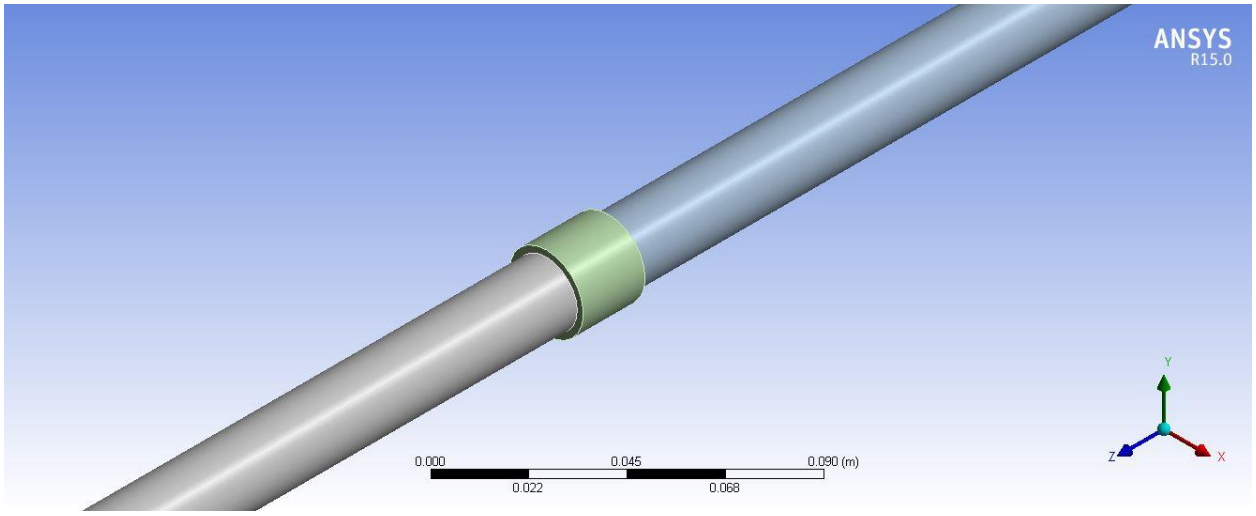

Fig. 3.6: Incident Bar , Specimen(D=24mm) & Transmitting Bar in Ansys Window

- L = 20mm and D =28 mm

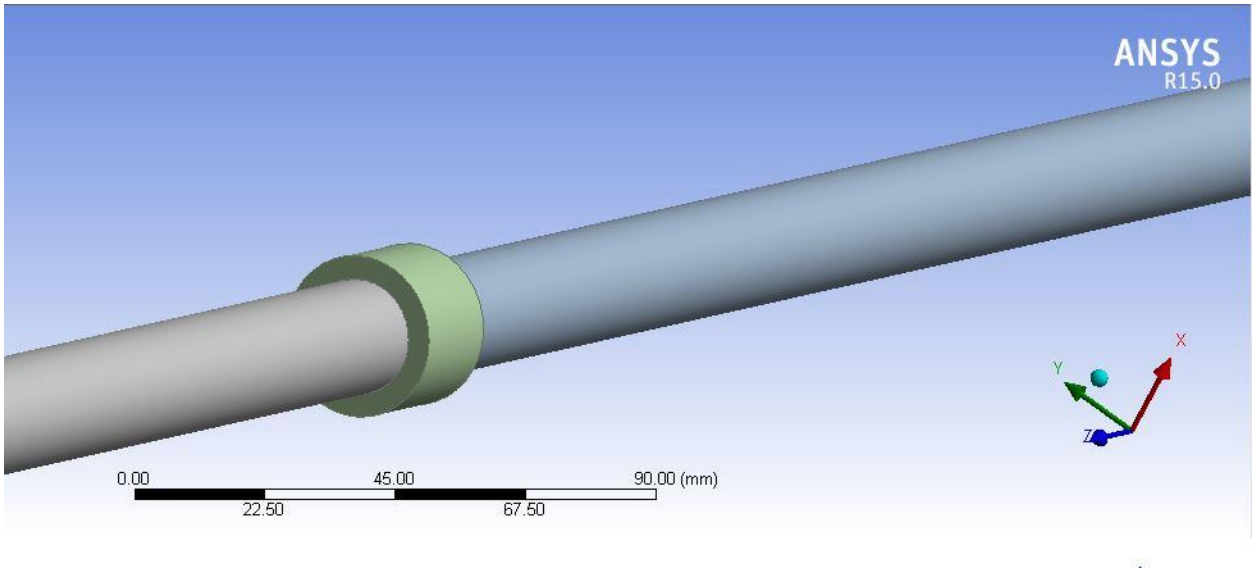

Fig. 3.7: Incident Bar , Specimen(D=28mm) & Transmitting Bar in Ansys Window

- L = 20mm and D = 32mm

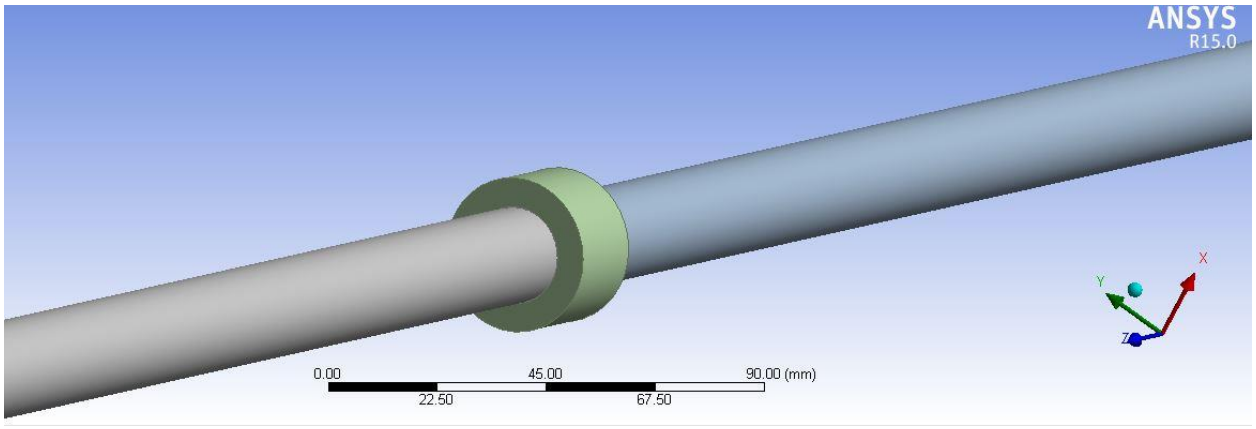

Fig. 3.8: Incident Bar , Specimen(D=32mm) & Transmitting Bar in Ansys Window

2. Meshing

Four node hexahedral elements with inflation set as smooth transition control are used for meshing the incident bar, transmission bar and the alloy sample. Edge sizing and multi zone methods were used to make the mesh even throughout the geometry.

- L=D=20 mm

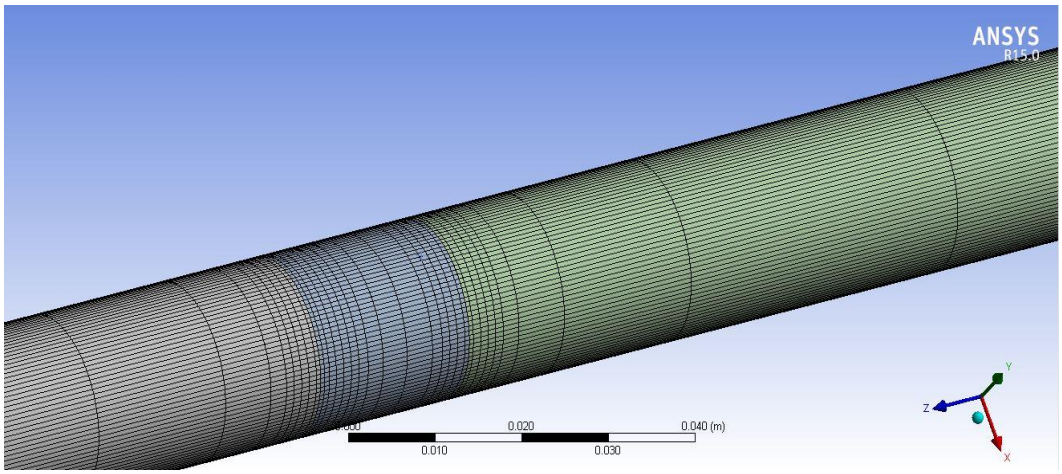

(a)

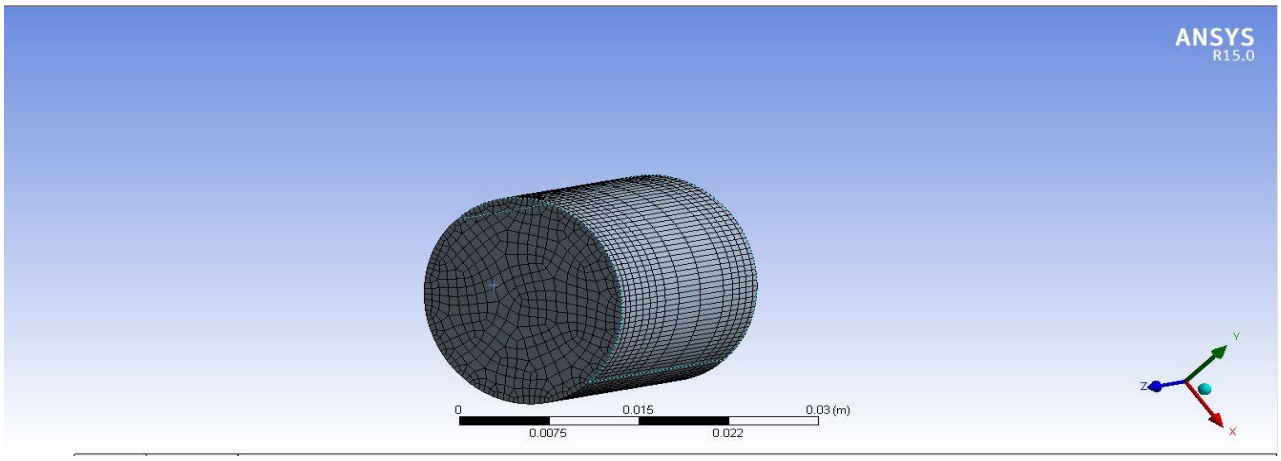

(b)

Fig. 3.9: (a) Meshing at Incident bar, transmitting bar and Specimen Interface, (b) Meshing on the Specimen

The incident bar is meshed to 24157 Elements, Specimen bar is meshed to 7305 Element and Transmitting Bar is meshed to 24157 Elements.

- L = 20mm, D = 24 mm

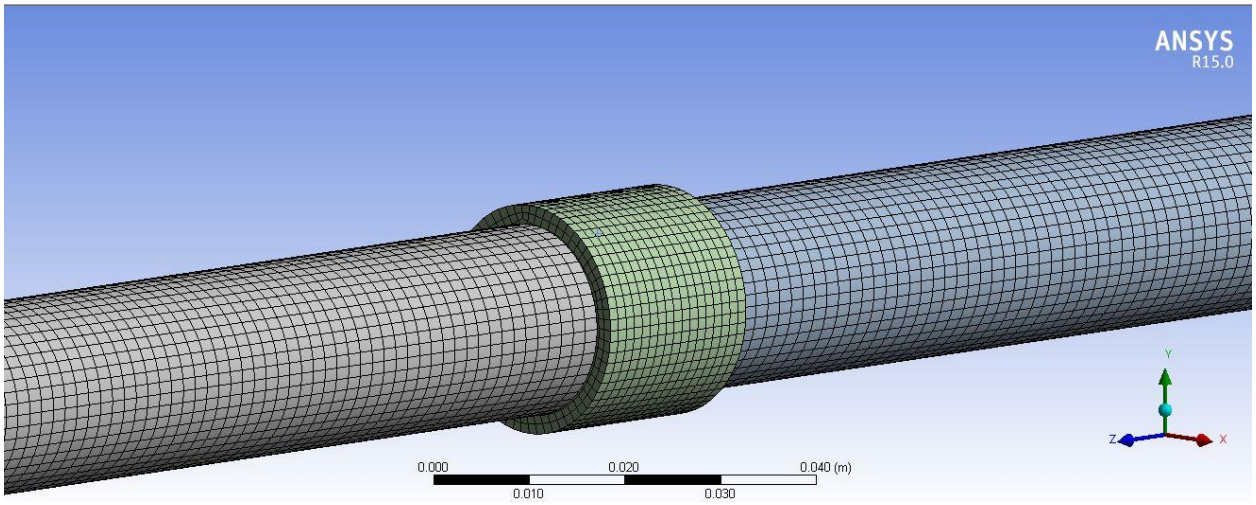

Fig.3.10: Meshing at Incident bar, transmitting bar and Specimen Interface(L=20mm and D=24mm)

The incident bar is meshed to 65128 Elements, Specimen bar is meshed to 17305 Element and Transmitting Bar is meshed to 65128 Elements.

- L=20 mm and D = 28 mm

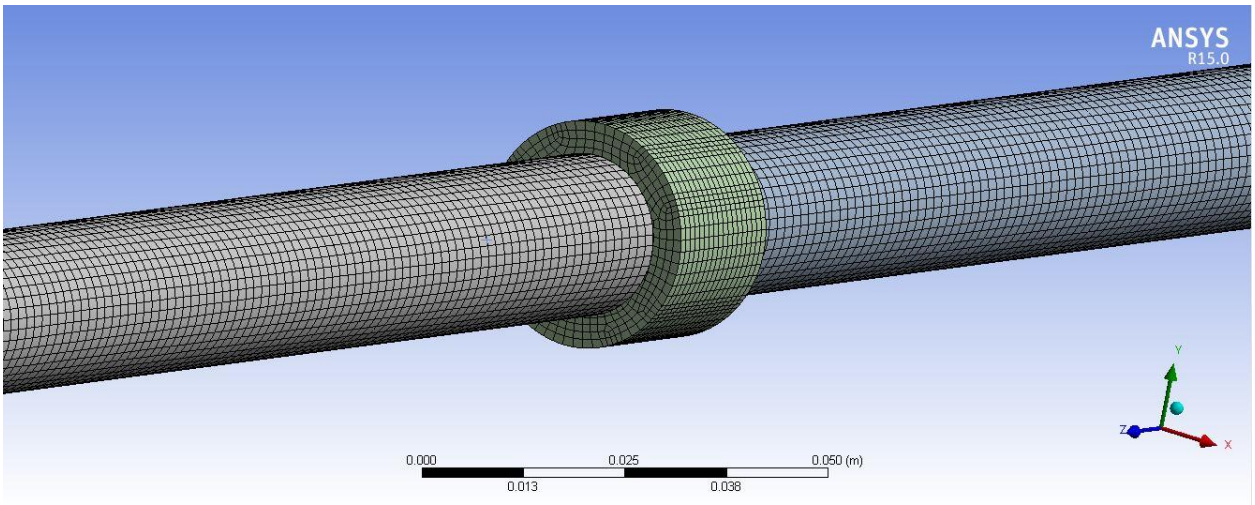

Fig. 3.11: Meshing at Incident bar, transmitting bar and Specimen Interface(L=20mm and D=28mm)

The incident bar is meshed to 65128 Elements, Specimen bar is meshed to 25011 Elements and Transmitting Bar is meshed to 65128 Elements.

- L=20 mm and D = 32mm

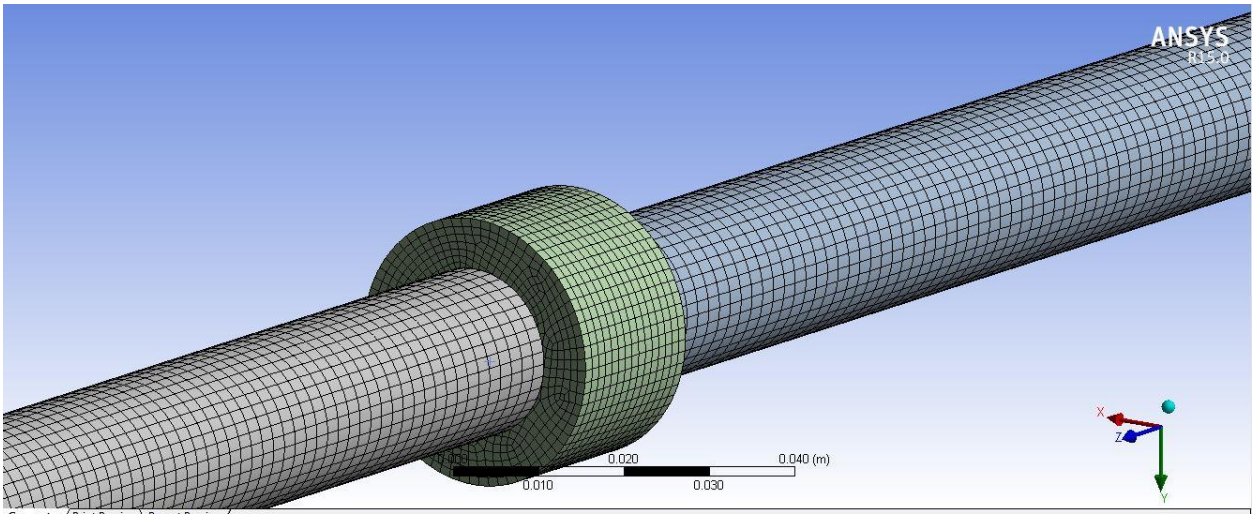

Fig. 3.12: Meshing at Incident bar, transmitting bar and Specimen Interface(L=20mm and D=32mm)

The incident bar is meshed to 65128 Elements, Specimen bar is meshed to 31065 Elements and Transmitting Bar is meshed to 65128 Elements.

Table 2: Number of Element in each part for all L-D combinations

Part \ L-D	20-20	20-24	20-28	20-32
Incident Bar	24157	65128	65128	65128
Specimen	7305	17305	25011	31065
Transmitting Bar	24157	65128	65128	65128

3. Interaction between the parts

Hard is taken as the interaction property between specimen and bar interface, and sample and bar contact is taken as frictionless

Boundary conditions

- The end of the transmission bar is kept fixed. For allowing one dimensional propagation of wave boundary condition are applied accordingly. The uniaxial simulations are performed for Aluminum alloy.
- A unidirectional impact force of 27kN was applied at the end of Incident Bar.

Chapter 4 Research and Discussion

4.1 Introduction

In this chapter the proposed simulation model and developed solution methodology was implemented to examine the stress-strain relation of the Aluminum alloy(LM-13) under high strain loading for two cases of four combinations of length and diameter of specimen first Length was kept 20 mm, Diameter was varied from 20-24mm. In the second case length was kept at 24mm and diameter was varied. Stress-strain data was obtained after simulations conducted on ANSYS. The effects of increment in diameter were investigated. The aptness of simulation is ensured by comparing with the existing results available in the literature and comparing with experimental data recorded at Terminal Ballistic Research Laboratory(TBRL)-DRDO, Chandigarh.

4.2 Strain Analysis of aluminum with different L/D ratio

Three specimens of each material of L/D ratio = 0.5, 1.0 and 1.5 were tested experimentally and through simulation. The results of the simulation were verified using experimental data. The specimens were divided in groups of three i.e., Aluminum, Copper and Steel. These three were further sub-divided in the group of Three L/D ratios i.e., 0.5, 1 and 1.5.

4.2.1 Comparison of F.E Analysis and SHPB Experimental data of Aluminum for L/D = 0.5

The Specimen was impacted with the force of 29KN for $2x10^{-4}$s. Stress-strain graph was recorded for the Experimental and Simulation data.

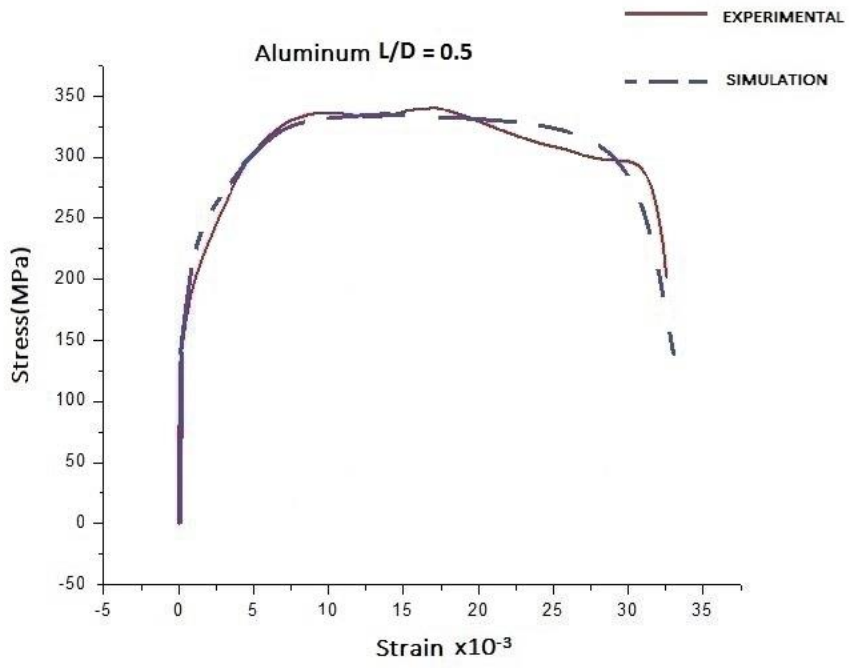

Fig. 4.1 Stress-strain plot for aluminum L/D = 0.5

4.1.2 Comparison of F.E. analysis and SHPB data for Aluminum for L/D =1.0

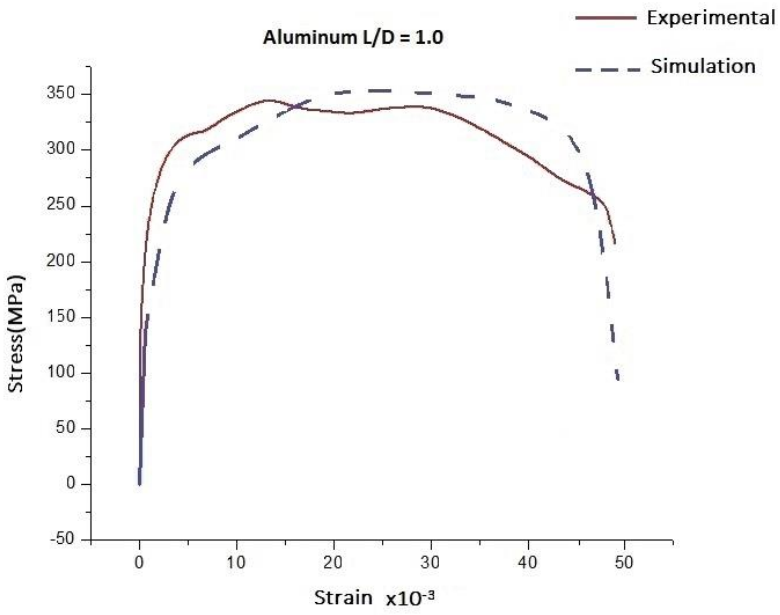

Fig. 4.2: Stress-Strain plot for Aluminum L/D =1.0

Specimen was made to strike with a force of 33KN for a time duration of $2x10^{-4}$s.

4.1.3 Comparison of F.E Analysis and SHPB Experimental data of Aluminum for L/D = 1.5

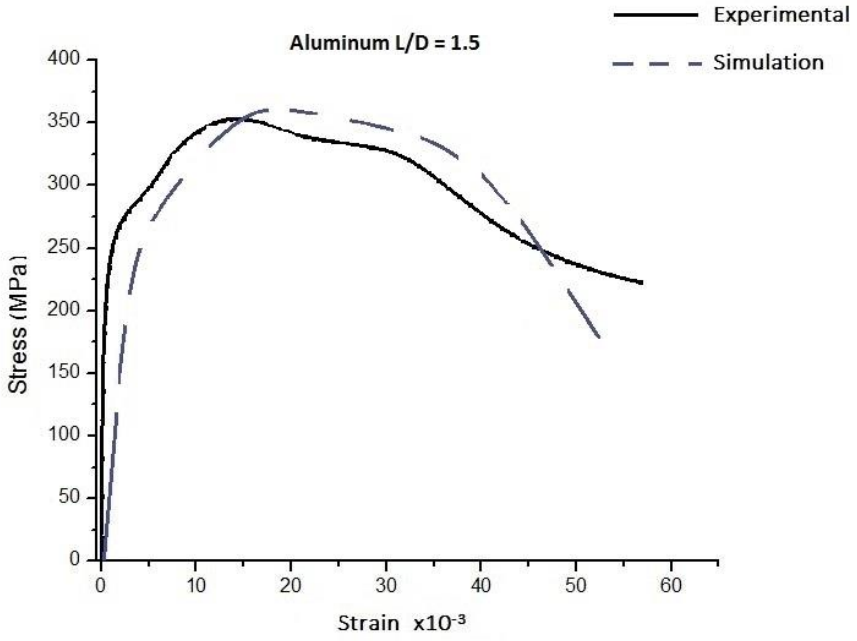

Fig. 4.3: Stress-Strain plot for Aluminum L/D =1.5

The striker was made to hit with force of 39KN for a duration of $2x10^{-4}$s.

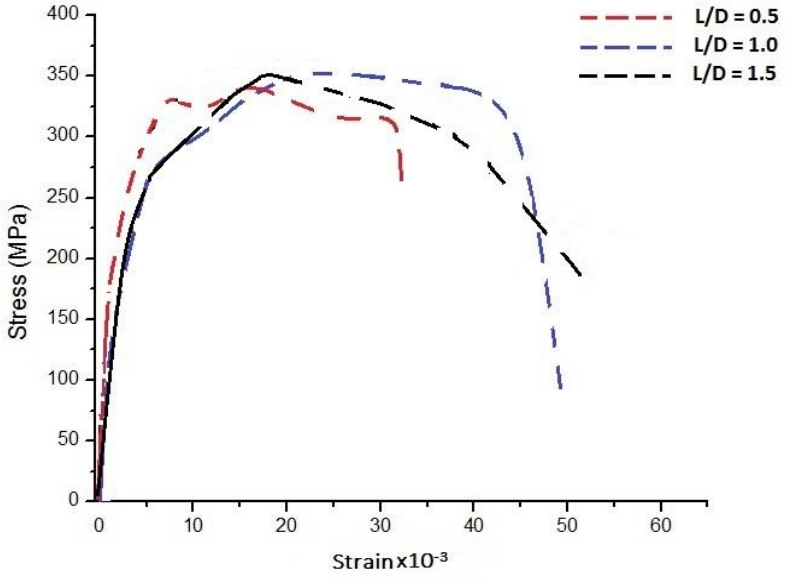

Fig. 4.4: Comparison plot for aluminum samples

It can be seen from figure 4.4 that strain and stress of the three specimens (i.e., L/D =0.5,1 &1.5) is following a particular trend with increase in the diameter of the sample (i.e., from 3.56 to 8.5mm). It was observed that increase in diameter there is continuous decrease in strain .

However in these samples length is not similar. Detailed specification of the samples are shown in the table 3.

Table 3: L/D specification for the aluminum samples

L(mm)	4.5	8.03	8.03
D(mm)	8.5	8.03	3.56
L/D	0.5	1.0	1.5

4.3 Strain rate analysis of copper with different L/D ratios

4.3.1 Comparison of F.E analysis and SHPB experimental data of Copper for L/D =0.5

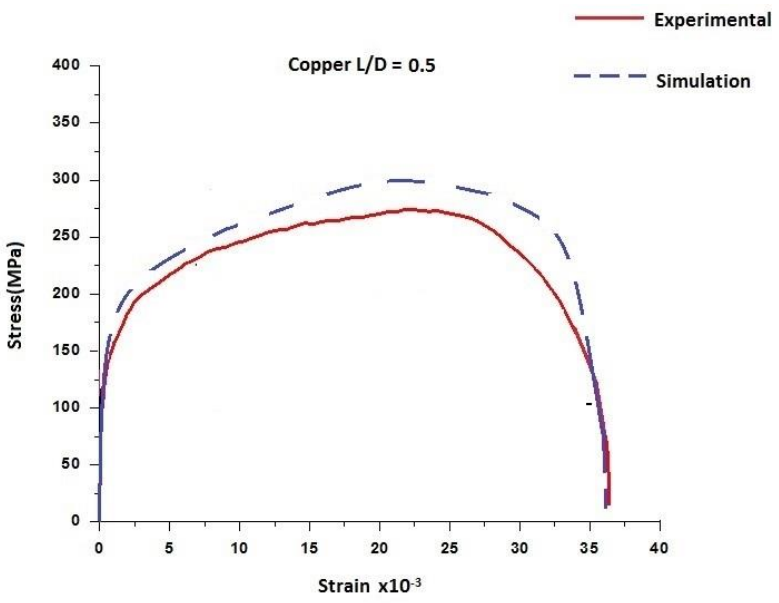

Fig. 4.5 Stres-strain plot for copper L/D =0.5

Copper specimen with L/d ratio = 0.5 was hit with the force of 28KN for time $2x10^{-4}$s.

4.3.2Comparison of F.E analysis and SHPB experimental data of Copper for L/D =1.0

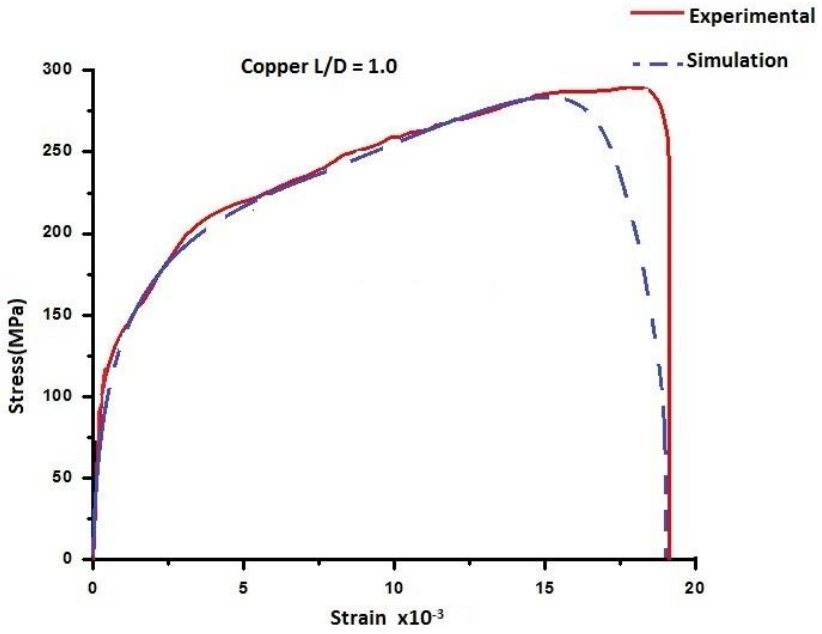

Fig. 4.6: Stress-strain plot for Copper L./D =1.0

Force on L/D ratio 1.0 specimen was 32kN for time $2x10^{-4}$s.

4.3.3Comparison of F.E analysis and SHPB experimental data of Copper for L/D = 1.5

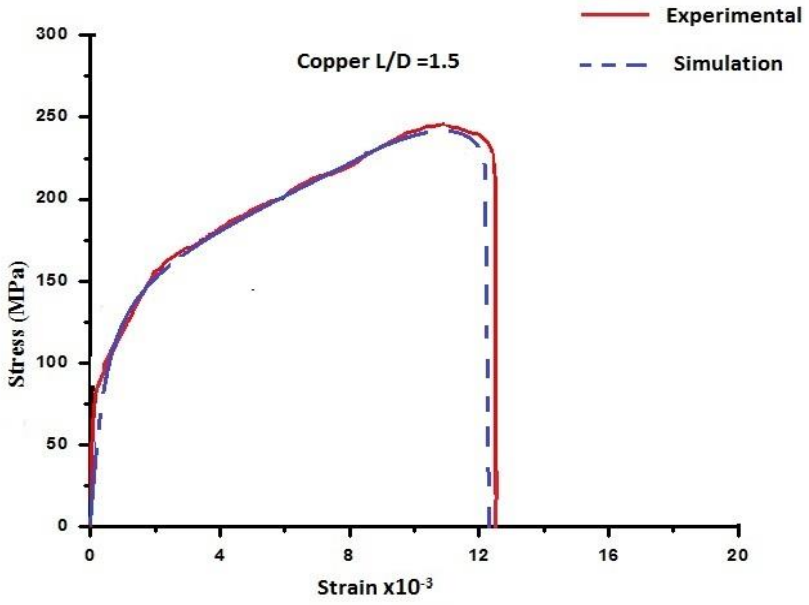

Fig. 4.7: Stress-strain plot for Copper L/D =1.5

Force on the specimen was 39kN for time duration $2x10^{-4}$.

The stress strain graph of all the three samples is shown in figure 4.8.

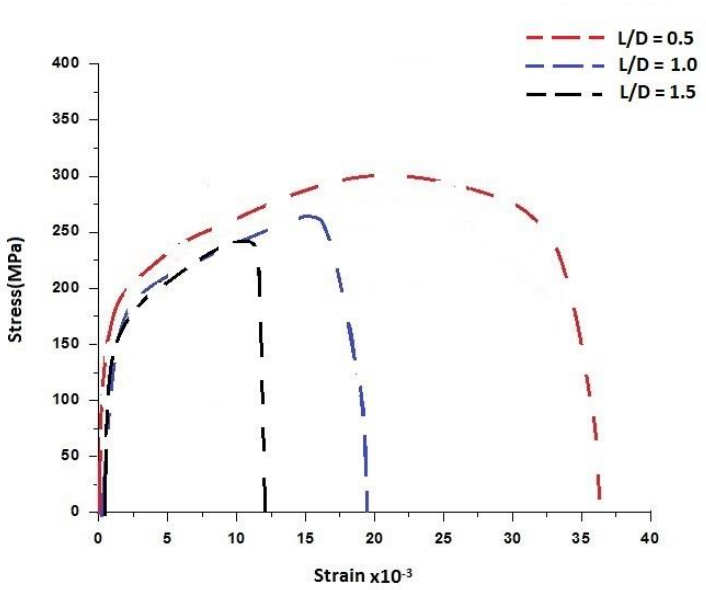

Fig. 4.8 Comparison plot for copper samples

The detailed specification of the three copper samples is shown in table 4.

Table 4: L/D specification of the three copper samples

L(mm)	8.03	8.03	8.03
D(mm)	16.05	8.03	5.33
L/D(mm)	0.5	1.0	1.5

It can be clearly seen that strain of the sample with maximum diameter is highest among the three sample. Strain rate goes on decreasing with decrease in diameter of the test sample. The length of the samples was taken same and diameter is varied to maintain the L/D ratio of 0.5, 1.0 and 1.5.

4.4 Strain rate analysis of steel with different L/D ratios

4.4.1 Comparison of F.E analysis and SHPB experimental data of steel for L/D = 0.5

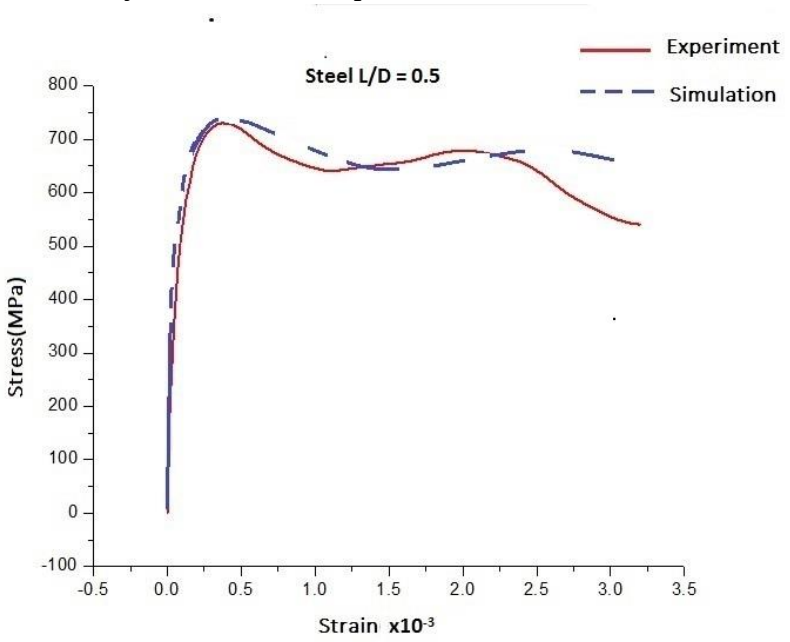

Fig. 4.9: Stress-Strain plot for Steel L/D =0.5

Steel specimen with L/d ratio = 0.5 was hit with the force of 28KN for time $2x10^{-4}$s.

4.4.2 Comparison of F.E analysis and SHPB experimental data of steel for L/D = 1.0

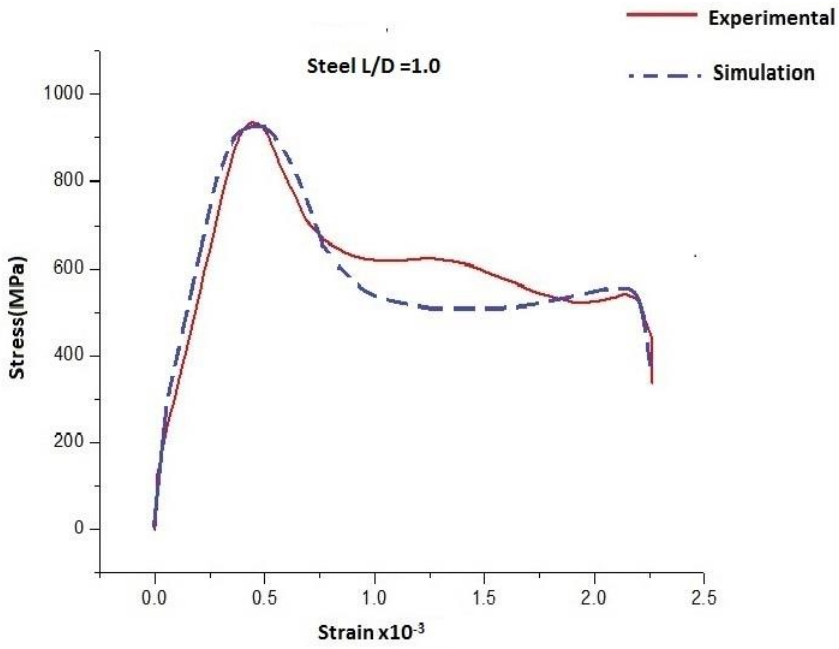

Fig. 4.10: Stress-strain plot for Steel L/D =1.0

Force on L/D ratio 1.0 specimen was 32kN for time $2x10^{-4}$s.

4.4.3Comparison of F.E analysis and SHPB experimental data of steel for L/D = 1.5

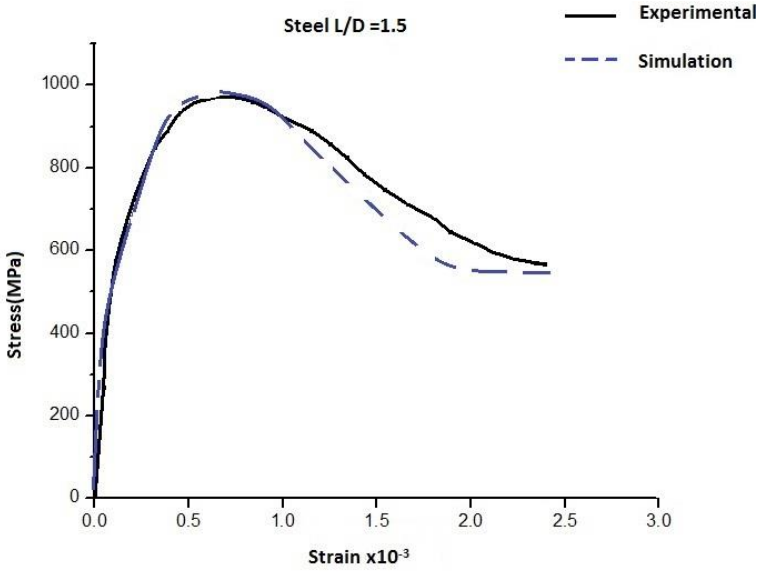

Fig. 4.11: Stress-strain plot for Steel L/D = 1.5

Force on the specimen was 39kN for time duration $2x10^{-4}$ s. Figure 4.11 is showing stress vs strain graphs for all the three steel samples.

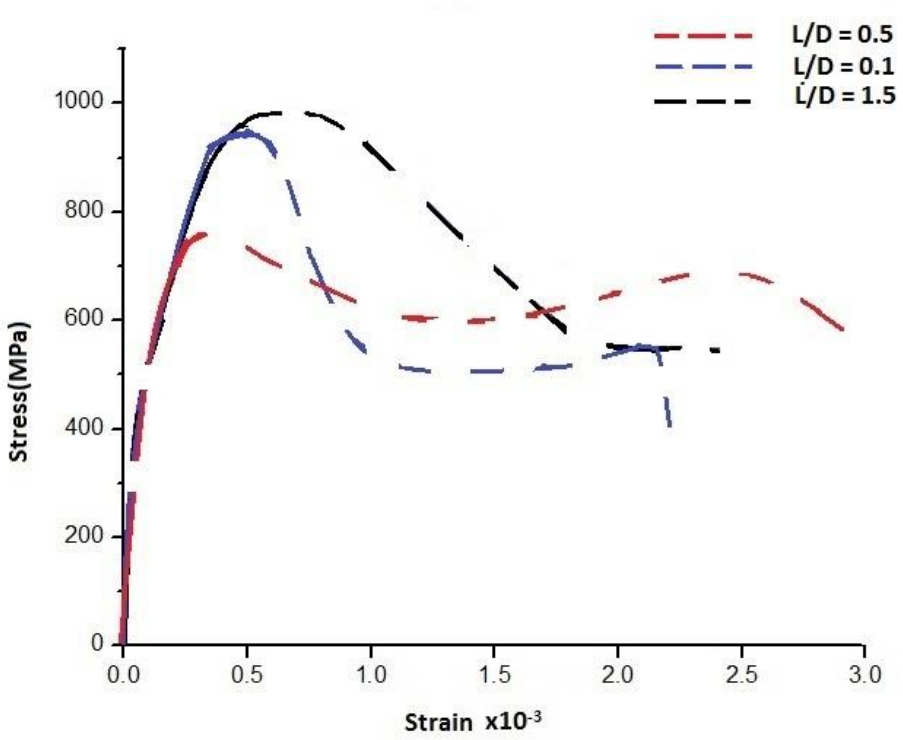

Fig. 4.12: Comparison plot for streel samples

It is observed from the figure that sample with highest diameter shows maximum strain. Strain goes on decreasing with decrease in sample diameter. In this case also, length of samples is kept same and diameter is varied to maintain the L/D ratio.

4.5 High strain analysis of Al_2O_3 MMCs

In order to validate the present results, a problem from Aradhayeet al.(2017) was solved using present methodology. Aradhaye et al. conducted the high strain impact on A356/Al_2O_3 metal matrix composites (MMCs) reinforced with 0%, 4%, 8% and 12% fiber volume fraction of Al_2O_3.For validation, stress-strain characteristics MMC with 0% has been studied. In the literature, the length and diameter of the incident and transmitting bar are taken 750mm each and of specimen, 10 and 12mm respectively.

Table 5: Dimensions of the Parts of SHPB in the Aradhye et al.(2017).

	Incident Bar	Specimen	Transmitting Bar
Length(mm)	750	10	750
Diameter(mm)	750	12	750

The SHPB setup was modelled according to the boundary conditions given in the literature .

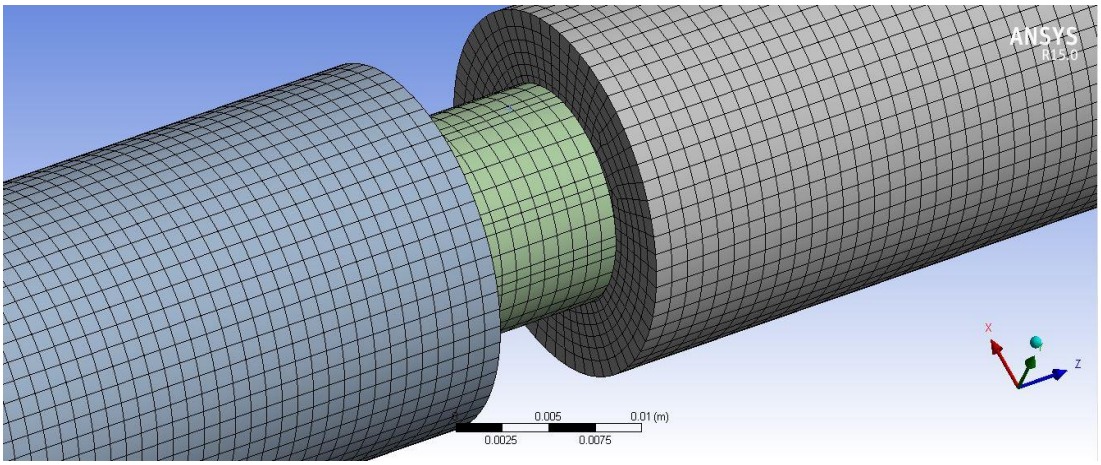

Fig. 4.13: Meshing of the model

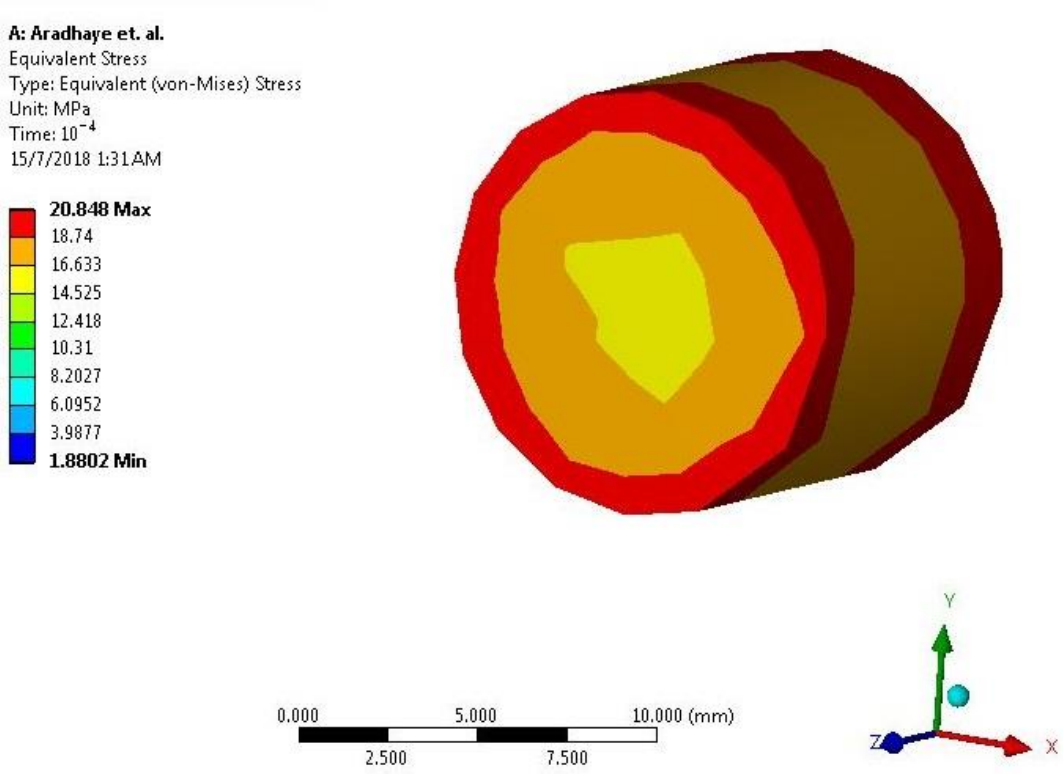

Fig. 4.14: Stress contour diagrams for specimen after impact

The SHPB setup was modelled in accordance to the literature. Incident and Transmitted Bar was meshed with 44359 elements and specimen with 2345 elements. The maximum value of the stress and strain in the specimen was found to be 20.848 MPa as shown in figure 4.14.

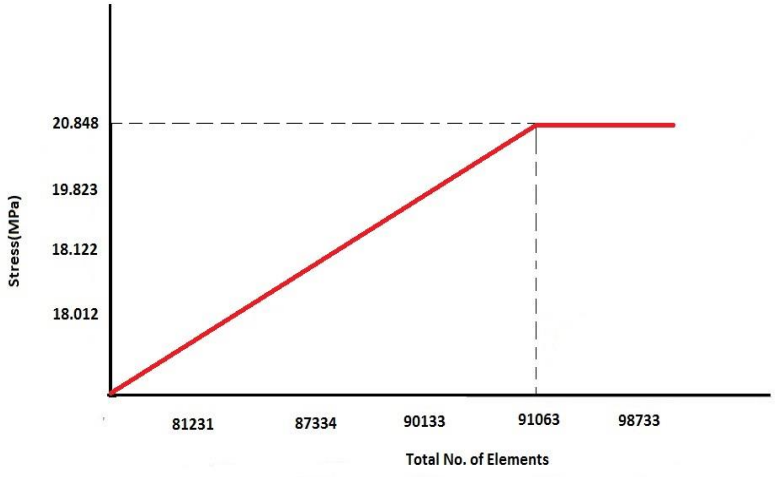

Fig 4.15: Mesh Convergence Plot

It was observed that after 91063 elements there was no significant change in the stress values as shown in figure 4.15.

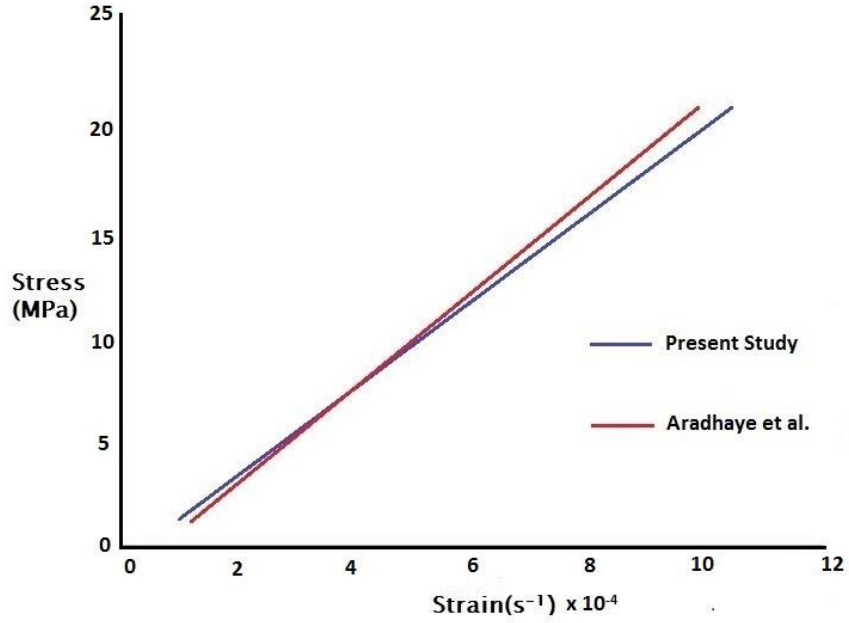

Fig. 4.16: Stress vs strain rate plot comparing the present study and Aradhaye *et al*.(2017)

Figure 4.16 shows stress vs strain plot of the present study and Aradhaye *et al*. It can be seen that the result given by the simulation agree accordingly with that of literature.

4.6 High strain Analysis of Aluminum Alloy(LM-13)for large diameters

For observing the high strain impact for diameters greater than 20mm, two cases were taken. First, four cylindrical model of LM-13 specimen were simulated on ANSYS by keeping length at 20mm and increasing diameter from 20-32mm. In the second case, length was increased to 24mm and diameter was again varied from 20mm to 32mm. So, in total 8 cases were simulated and strain-rate was recorded. In both the cases the impact stress was taken as 105MPa in accordance to the experiments conducted at TBRL, DRDO. Time duration was set as $2x10^{-4}$s.

4.6.1 F.E analysis of Al(LM-13) For L=20mm and D = 20,24,28,32mm

The diameter is varied and the length is kept constant at 20mm. The specification of the test samples of LM-13 are shown in table 7.

Table 6: L/D ratio specification for D=20mm

L(mm)	20	20	20	20
D(mm)	20	24	28	32
L/D	1.0	0.833	0.714	0.625

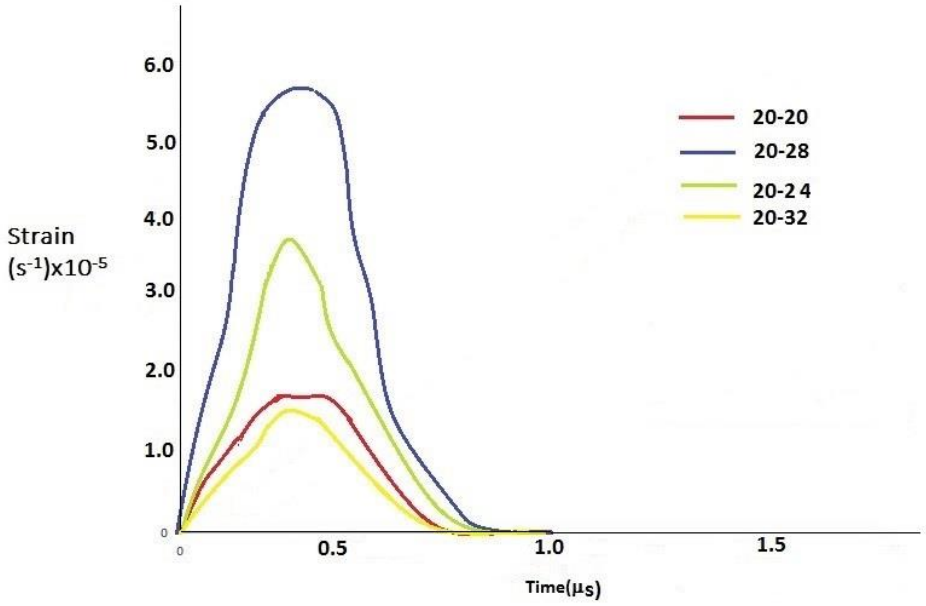

Fig 4.17: Strain vs time plot for L = 20mm and D = 20-32

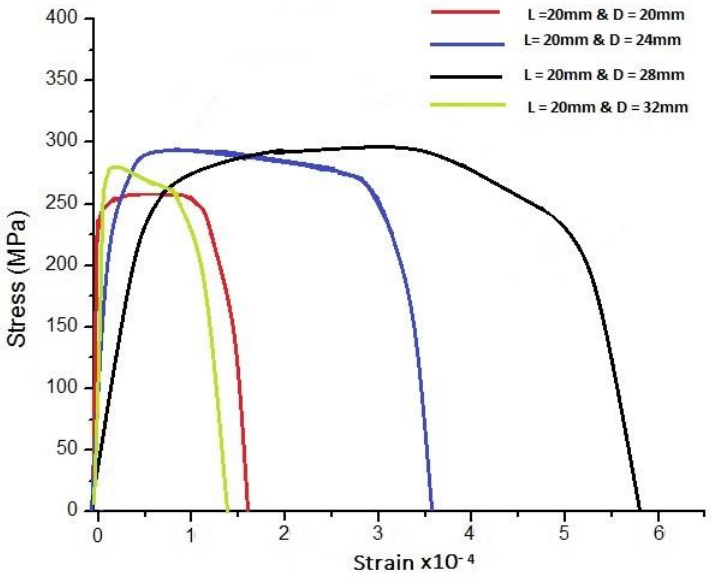

Fig. 4.18: Stress-strain plot for L= 20mm and D= 20-32mm

Figure 4.18 is showing stress vs strain graph of all the LM-13 samples with 20 mm length, it can be observed that with increase in diameter there is respective increase in strain. The maximum stress remains nearly same. Samples of LM-13 also depicts the same trend of increasing strain rate as shown by copper and steel with similar pattern of length and diameter. However, samples with highest diameter (i.e., D = 32mm) did not lie within the trend. This may be due to very large diameter as compared to the diameter of incident and transmitting bars.

4.6.2 F. E analysis of Aluminum alloy (LM-13) For L=24mm and D = 20,24,28,32mm
The diameter is varied and the length is kept constant at 24mm. The specification of the test samples of LM-13 are shown in table 8.

Table 7: L/D ratio specification for L=24mm

L	24	24	24	24
D	20	24	28	32
L/D	1.2	1.0	0.857	0.75

The Length is kept constant at 24mm and diameter is varied from 20-32mm.

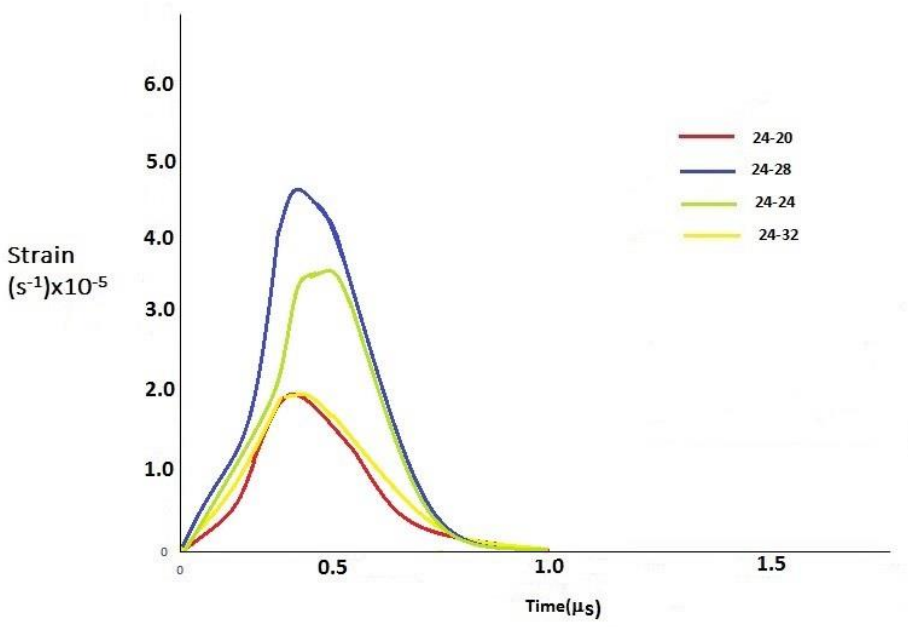

Fig. 4.19: Strain vs time plot for L=24mm and D=20-32mm

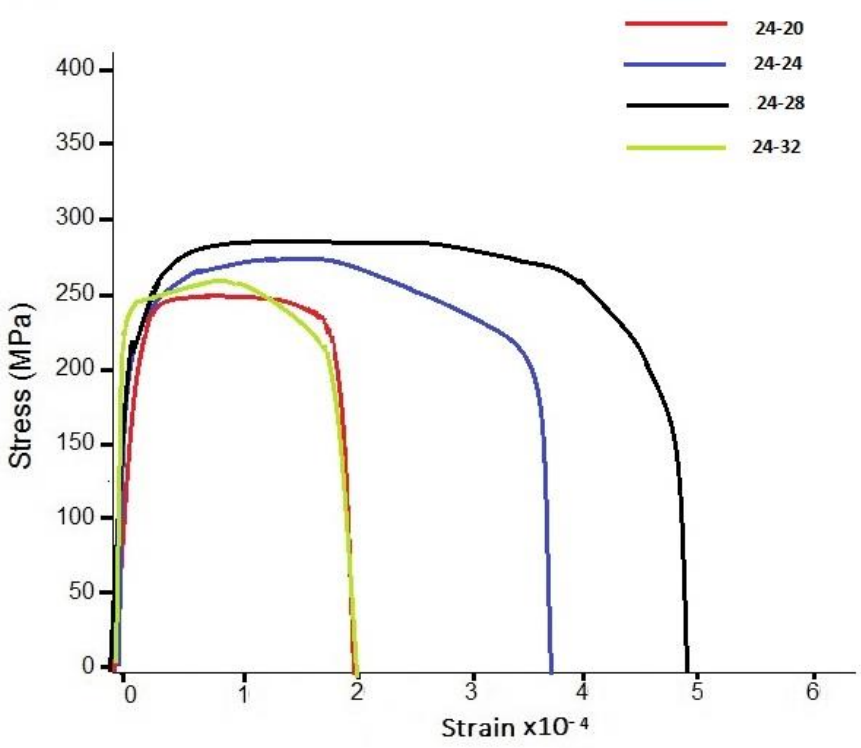

Fig. 4.20: Stress-strain plot for L=24mm and Diameter = 20-32mm

Stress vs strain graphs of four LM-13 sample having 24mm length and varying diameter is shown in figure 4.20. It is clearly observed that strain rate increases with increase in diameter. Although, the length of the sample remains unchanged, the trends of increasing strain rate is not following by the sample with 32mm diameter. Very large diameter sample in comparison to the diameter of incident and transmitting may be the possible reason of varying result.

4.7 Discussion

In sections 4.2 to 4.4, Simulation results were validated with Experimental results. It was observed that the both the results were in agreement. In section 4.5, a problem for literature is simulated and a close agreement between the results of simulation and presented in literature was observed. Maximum stress and strain rate in the literature was 20.192 MPa and 0.001 s respectively. In the present study, the maximum stress was found to be 20.848 MPa and strain 0.0012 s. In section 4.6, two sets of combination of specimen were simulated Keeping L= 20mm and changing D = 20-24mm. It was observed that there is a rise in strain rate from 20-28mm with maximum strain as $5x10^{-5}$ but as the diameter is further increased to 32mm there is no significant decrement in strain rate. It can be stated that up to diameter 28mm there will be increase in strain rate but after that there would be no change in strain rates Keeping L =24mm and changing D =

20-24mm. It was observed that maximum strain of 4.7 $x10^{-5}$ was observed at D = 28mm and minimum for D =32mm as $4.5x10^{-5}$. It can be observed from the trend of increasing strain shown by samples of aluminum, copper, steel, LM-13(20mm) and LM-13(24mm) that strain increases with increase in diameter but length is kept constant. Whereas, samples of Al with varying diameter as well as length, did not produce any expected trend as shown by other samples. Samples of Aluminum, copper and steel are having diameters less than the incident and transmitting bar (i.e., 20mm). The trend shown by the simulated results of the samples of LM-13(20mm) and LM-13(24mm) clearly gave useful information that samples with diameter larger than the diameter of incident bar and transmitting bar followed the same trend as followed by copper and steel. The trend is proven confident for larger diameter i.e., up to 40mm more than the diameter of incident bar and transmitting bar. It can be well stated that simulated results of samples with diameter larger than the diameter of transmitting bar and incident bar can be well accepted without performing experiments on different setup with large diameter incident bar and transmitting bar. This provides more flexibility to accept large variety of sample on same machine with minimum cost.

Chapter 5 Conclusion and Future scope

5.1 Conclusion

As is observed that results obtained through simulation and experiments are in good agreement with other. Simulated results are also in good agreement with experimental results presented in literature. There are few important conclusions made from the present study which are as follows:

- Samples with diameter larger than the diameter of incident bar and transmitting bar can be tested through F.E. analysis.
- Sample diameter should not be more than 40% of the diameter of incident/transmitting bar.
- For varying diameter, the length of the sample should remain same
- Methodology used in the present study eliminates the need of different machines required for different samples upto certain limit

5.2 Future Scope

Present study gives good result for soft metal and alloy. Similar study can also be carried out for ceramics and carbides such as tungsten carbides. There is need to estabilish a database of simulated for different materials so that cost and time involved in experimentation can be greatly reduced. More researcher may be benefitted from the database without having costly setup of Split Hopkinsons Pressure Bar.

References

H. Kolsky, "An Investigation of the Mechanical Properties of Materials at very High Rates of Loading," *Proceedings of the Physical Society. Section B*, vol. 62, no. 11, pp. 676–700, Jan. 1949.

B.P. Hughes and R. Gregory, "Concrete subjected to high rates of loading in compression," *Magazine of Concrete Research*, vol. 24, no. 78, pp. 25–36, 1972.

W. Chen and G. Ravichandran, "Dynamic compressive failure of a glass ceramic under lateral confinement," *Journal of the Mechanics and Physics of Solids*, vol. 45, no. 8, pp. 1303–1328, 1997.

O. Lee and M. Kim, "Dynamic material property characterization by using split Hopkinson pressure bar (SHPB) technique," *Nuclear Engineering and Design*, vol. 226, no. 2, pp. 119–125, 2003.

S. G. Grantham, C. R. Siviour, W. G. Proud, S. M. Walley, and J. E. Field, "Speckle measurements of sample deformation in the split Hopkinsons pressure bar," *Journal de Physique IV (Proceedings)*, vol. 110, pp. 405–410, 2003.

W. W. Chen, A. M. Rajendran, B. Song, and X. Nie, "Dynamic Fracture of Ceramics in Armor Applications," *Journal of the American Ceramic Society*, vol. 90, no. 4, pp. 1005–1018, 2007.

M. Güden, A. Taşdemirci, and Ç. Ergönenç, "Split Hopkinson pressure bar multiple reloading and modeling of a 316 L stainless steel metallic hollow sphere structure," *International Journal of Impact Engineering*, vol. 37, no. 3, pp. 250–259, 2010.

D. J. Kim, K. Sirijaroonchai, S. El-Tawil, and A. E. Naaman, "Numerical simulation of the Split Hopkinson Pressure Bar test technique for concrete under compression," *International Journal of Impact Engineering*, vol. 37, no. 2, pp. 141–149, 2010.

Y. Chen, A. Clausen, O. Hopperstad, and M. Langseth, "Application of a split-Hopkinson tension bar in a mutual assessment of experimental tests and numerical predictions," *International Journal of Impact Engineering*, vol. 38, no. 10, pp. 824–836, 2011.

S. Wang, M.-H. Zhang, and S. T. Quek, "Mechanical behavior of fiber-reinforced high-strength concrete subjected to high strain-rate compressive loading," *Construction and Building Materials*, vol. 31, pp. 1–11, 2012.

H. Su and J. Xu, "Dynamic compressive behavior of ceramic fiber reinforced concrete under impact load," *Construction and Building Materials*, vol. 45, pp. 306–313, 2013.

J. Kajberg and K. Sundin, "High-Temperature Split-Hopkinson Pressure Bar with a Momentum Trap for Obtaining Flow Stress Behaviour and Dynamic Recrystallisation," *Strain Journal*, vol. 50, no. 6, pp. 547–554, 2014.

H. Su, J. Xu, and W. Ren, "Mechanical properties of ceramic fiber-reinforced concrete under quasi-static and dynamic compression," *Materials & Design*, vol. 57, pp. 426–434, 2014.

S. Daniel, "A Study on the behaviour of Aluminium alloy (LM13) reinforced with NanoZrO2Particulate," *IOSR Journal of Engineering*, vol. 4, no. 2, pp. 58–62, 2014.

Babu C. V., Rao V.K.V (2014), Behaviour of M30 Grade concrete with confinement under axial compression, International Journal of Engineering Research and Applications, ISSN: 2248-9622, Vol-4, Issue 9(version-5), pp.75-80

Y. Al-Salloum, T. Almusallam, S. Ibrahim, H. Abbas, and S. Alsayed, "Rate dependent behavior and modeling of concrete based on SHPB experiments," *Cement and Concrete Composites*, vol. 55, pp. 34–44, 2015.

F. Lu, Y. Lin, X. Wang, L. Lu, and R. Chen, "A theoretical analysis about the influence of interfacial friction in SHPB tests," International Journal of Impact Engineering, vol. 79, pp. 95–101, 2015.

Adrian R., Mihai B., and Tudor C., "Finite element methods in split hopkinsons pressure bar developing process." *International Journal of Impact Engineering*, vol. 57.3, pp. 263-268, 2016.

K.H. Nguyen, H. C. Kim, H. Shin, Y.-H. Yoo, and J.-B. Kim, "Numerical investigation into the stress wave transmitting characteristics of threads in the split Hopkinson tensile bar test," *International Journal of Impact Engineering*, vol. 109, pp. 253–263, 2017.

S. Nawale, R. Vyavahare, and A. Aradhye, "High Strain Rate Response of A356/Al_2O_3 Aluminum Alloy MMCs Using Ls-Dyna," *Procedia Engineering*, vol. 173, pp. 1967–1974, 2017.

Q. Hu, F. Zhao, H. Fu, K. Li, and F. Liu, "Dislocation density and mechanical threshold stress in OFHC copper subjected to SHPB loading and plate impact," *Materials Science and Engineering: A*, vol. 695, pp. 230–238, 2017.

F. Lu, Y. Lin, X. Wang, L. Lu, and R. Chen, "A theoretical analysis about the influence of interfacial friction in SHPB tests," International Journal of Impact Engineering, vol. 79, pp. 95–101, 2015.

S. Mishra, T. Chakraborty, and V. Matsagar, "Dynamic Characterization of Himalayan Quartzite using SHPB," *Procedia Engineering*, vol. 191, pp. 2–9, 2017.

B.P. Hughes and R. Gregory, "Concrete subjected to high rates of loading in compression," *Magazine of Concrete Research*, vol. 24, no. 78, pp. 25–36, 1972.

D. Braess, *Finite elements: theory, fast solvers, and applications in solid mechanics*. Cambridge: Cambridge University Press, 2007.

N. S. Gokhale, S. S. Deshpande, S. V. Bedekar, and A. N. Thite, *Practical finite element analysis*. Pune: Finite To Infinite, 2008.

Document Viewer

Turnitin Originality Report

Processed on: 29-Jul-2018 20:20 +0530
ID: 985979146
Word Count: 8578
Submitted: 1

Anmol 5 By Anmol 5

Similarity Index	Similarity by Source	
15%	Internet Sources:	7%
	Publications:	10%
	Student Papers:	5%

include quoted include bibliography excluding matches < 8 words download refresh print

mode: quickview (classic) report

2% match (Internet from 29-Dec-2017)
http://ethesis.nitrkl.ac.in

2% match (student papers from 31-May-2015)
Submitted to National Institute of Technology, Rourkela on 2015-05-31

1% match (publications)
Sunita Mishra, Tanusree Chakraborty, Vasant Matsagar. "Dynamic Characterization of Himalayan Quartzite using SHPB", Procedia Engineering, 2017

1% match (publications)
Qiushi Hu, Feng Zhao, Hua Fu, Kewu Li, Fusheng Liu. "Dislocation density and mechanical threshold stress in OFHC copper subjected to SHPB loading and plate impact", Materials Science and Engineering: A, 2017

1% match (publications)
Dyab, Mohamad, Payam Matin, and Yuanwei Jin. "Finite Element Simulation for Design Verification of a Small Size Split Hopkinson Pressure Bar", Volume 2A 33rd Computers and Information in Engineering Conference, 2013.

1% match (publications)
D. J. Frew. "A split Hopkinson pressure bar technique to determine compressive stress-strain data for rock materials", Experimental Mechanics, 03/2001

1% match (publications)
Fangyun Lu, Yuliang Lin, Xiaoyan Wang, Li Lu, Rong Chen. "A theoretical analysis about the influence of interfacial friction in SHPB tests", International Journal of Impact Engineering, 2015

1% match (publications)
A. Morales-Rodríguez, M. Jiménez-Melendo, A. Domínguez-Rodríguez, A. Bravo-León. "High-temperature plastic behavior of reaction-bonded CuO and TiO2 co-doped alumina–zirconia", Materials Science and Engineering: A, 2004

<1% match (publications)
S.P. Nawale, R.T. Vyavahare, A.S. Aradhye. "High Strain Rate Response of A356/Al 2 O 3 Aluminum Alloy MMCs Using Ls-Dyna", Procedia Engineering, 2017

<1% match (publications)
Haoyang Su, Jinyu Xu, Weibo Ren. "Mechanical properties of ceramic fiber-reinforced concrete under quasi-static and dynamic compression", Materials & Design, 2014

<1% match (publications)
Khac-Ha Nguyen, Hee Cheol Kim, Hyunho Shin, Yo-Han Yoo, Jong-Bong Kim. "Numerical investigation into the stress wave transmitting characteristics of threads in the split Hopkinson tensile bar test", International Journal of Impact Engineering, 2017

<1% match (student papers from 01-Jun-2015)
Submitted to National Institute of Technology, Rourkela on 2015-06-01